

# Accepted Manuscript

Design, synthesis, biological evaluation and molecular modeling of novel 1*H*-pyrazolo[3,4-*d*]pyrimidine derivatives as BRAF<sup>V600E</sup> and VEGFR-2 dual inhibitors

Yuanyuan Wang, Shanhe Wan, Zhonghuang Li, Yu Fu, Guangfa Wang, Jiajie Zhang, Xiaoyun Wu

PII: S0223-5234(18)30479-3

DOI: [10.1016/j.ejmech.2018.05.054](https://doi.org/10.1016/j.ejmech.2018.05.054)

Reference: EJMECH 10465

To appear in: *European Journal of Medicinal Chemistry*

Received Date: 11 April 2018

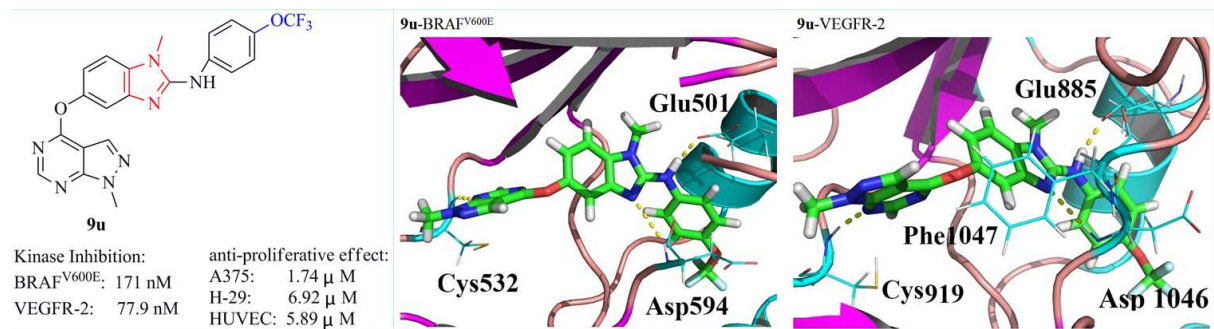
Revised Date: 30 May 2018

Accepted Date: 30 May 2018

Please cite this article as: Y. Wang, S. Wan, Z. Li, Y. Fu, G. Wang, J. Zhang, X. Wu, Design, synthesis, biological evaluation and molecular modeling of novel 1*H*-pyrazolo[3,4-*d*]pyrimidine derivatives as BRAF<sup>V600E</sup> and VEGFR-2 dual inhibitors, *European Journal of Medicinal Chemistry* (2018), doi: 10.1016/j.ejmech.2018.05.054.

This is a PDF file of an unedited manuscript that has been accepted for publication. As a service to our customers we are providing this early version of the manuscript. The manuscript will undergo copyediting, typesetting, and review of the resulting proof before it is published in its final form. Please note that during the production process errors may be discovered which could affect the content, and all legal disclaimers that apply to the journal pertain.





# Design, synthesis, biological evaluation and molecular modeling of novel 1*H*-pyrazolo[3,4-*d*]pyrimidine derivatives as BRAF<sup>V600E</sup> and VEGFR-2 dual inhibitors

Yuanyuan Wang<sup>1</sup>, Shanhe Wan<sup>1</sup>, Zhonghuang Li, Yu Fu, Guangfa Wang, Jiajie Zhang\*, Xiaoyun Wu\*

Guangdong Provincial Key Laboratory of New Drug Screening, School of Pharmaceutical Science, Southern Medical University, Guangzhou 510515, PR China

\*Corresponding author:

**E-mail:** zhangjj@smu.edu.cn (J.-J. Zhang), **Tel.:** +86-20-61648548;

**E-mail:** xywu@smu.edu.com (X.-Y. Wu), **Tel.:** +86-20-62789415.

<sup>1</sup> These authors contributed equally to this work.

## Abstract

Aiming to explore novel BRAF<sup>V600E</sup> and VEGFR-2 dual inhibitors, a series of 1*H*-pyrazolo[3,4-*d*]pyrimidine derivatives were designed, synthesized and biologically evaluated in this study. Most of the synthesized 1*H*-pyrazolo[3,4-*d*]pyrimidine compounds displayed moderate to high potent activity in both enzymatic and cellular proliferation assays. Among these compounds, **9e**, **9g**, **9m** and **9u** showed remarkably high inhibitory activities against both BRAF<sup>V600E</sup> and VEGFR-2 kinase comparable to positive control Sorafenib. Particularly, compound **9u** also showed potent anti-proliferative activity against BRAF<sup>V600E</sup>-expressing A375 (IC<sub>50</sub> = 1.74 μM) and H-29 (IC<sub>50</sub> = 6.92 μM) as well as VEGFR-2-expressing HUVEC (IC<sub>50</sub> = 5.89 μM), which was also comparable to Sorafenib. Furthermore, kinase selectivity profile showed that **9u** had almost poor or no significant inhibitory activity against wild-type BRAF and 15 other tested protein kinases. Flow cytometric analysis showed that compound **9u** mainly arrested the A375 and HUVEC cell lines in the G<sub>0</sub>/G<sub>1</sub> stage with a concentration-dependent effect. In addition, the molecular docking and molecular

dynamics simulations suggested that **9u** adopted a similar binding pattern with Sorafenib at the ATP-binding sites of BRAF<sup>V600E</sup> and VEGFR-2. Taken together, these results indicated that compound **9u** may serve as novel lead compound in research on more effective BRAF<sup>V600E</sup> and VEGFR-2 dual inhibitors.

**Keywords:** dual inhibitor; BRAF<sup>V600E</sup>; VEGFR-2; 1*H*-pyrazolo[3,4-*d*]pyrimidine; tyrosine kinase

## 1. Introduction

The mitogen activated protein kinase (MAPK) signaling pathway was the first signaling pathway elucidated from the cell surface receptors to the nucleus [1]. It consists of the RAS-RAF-MEK-ERK signal transduction cascade which is a vital driver of a number of cellular fates, including proliferation, differentiation and survival, making it an attractive pathway to target in several cancer types [2-4]. The RAF includes three subtypes of ARAF, BRAF and CRAF, and related studies have shown that the formation of complexes by these different isoforms has an important role in their activation [5-7]. BRAF isoform is more easily activated by RAS and has higher basal kinase activity than the other two isoforms, which provides a reasonable explanation for the mutational activation of BRAF frequently observed in human tumors. The most prevalent mutation of BRAF, accounting for more than 90% of the detected mutations in BRAF, is an amino acid substitution of glutamic acid for valine at residue 600 (V600E). The BRAF<sup>V600E</sup> mutation leads to constitutive kinase activity 500-700-fold greater than wild-type BRAF, which results in amplification of the MAPK pathway, and this mutation is most frequently associated with melanoma [8]. Besides, activating mutations are also present in a range of other human cancers, particularly thyroid (30%), colorectal (10%), and ovarian (35%) cancers [9]. Importantly, targeting this pathway, especially through inhibition of BRAF, is becoming more important in many current human cancer therapeutic approaches.

However, angiogenesis plays a crucial role in solid tumor progression because the tumors require significantly more oxygen, glucose, and other nutrients to sustain their rapid growth than do normal tissues [10]. Many cancer tissues secrete vascular endothelial growth factor (VEGF) to promote

angiogenesis from adjacent blood vessels [11]. The VEGFR-2 (VEGF receptor-2) is expressed on the surface of blood vessels, and it plays an important role in tumor angiogenesis. Its activation by VEGF initiates downstream signaling, ultimately leading to angiogenesis, vascular permeability enhancement, tumor proliferation, and tumor migration [11]. Inhibition of the VEGF signaling pathway has become a valuable approach in the treatment of cancers [12-16]. Therefore, targeting VEGFR-2 has been considered a rational approach for cancer treatment.

Moreover, recent studies showed that BRAF and VEGFR-2 have a certain synergistic effect on the occurrence and development of tumor [17-18]. Thus, the dual inhibition of BRAF<sup>V600E</sup> and VEGFR-2 represents a promising approach to cancer treatment. In recent years, some BRAF<sup>V600E</sup>/VEGFR-2 dual inhibitors have been approved or entered clinical trials, such as Sorafenib and RAF265. Sorafenib (Fig. 1) was developed as an inhibitor of multi-kinases, including tyrosine and serine/threonine kinases [19], and it has been launched for the treatment of renal cell carcinoma (RCC) and hepatocellular carcinomas (HCC) [20]. However, its lack of activity in metastatic melanoma phase 3 clinical trials may be because it shows insufficient RAF inhibition in melanoma tissues [21]. Another RAF inhibitor, RAF265 (Fig. 1), has also been reported as an RAF/VEGFR dual kinase inhibitor [22]. These two compounds are classified as type II inhibitors [23,24], which bind to and stabilize the DFG-out “inactive” conformation. They not only bind at the adenosine triphosphate (ATP) binding site, but also extend to the hydrophobic “back pocket” of protein created by the flip of the DFG motif. In contrast, Vemurafenib (PLX4032) [25-27] and Dabrafenib (GSK-2118436) (Fig. 1) [28] are classified as type I inhibitors, which bind to the DFG-in active conformation of the ATP binding site. These type I inhibitors of RAF are highly BRAF selective against other kinases, particularly VEGFR-2. Current researches illustrated that Vemurafenib and Dabrafenib cause rapid development of squamous cell carcinoma (SCC) and keratoacanthoma, which may be caused by paradoxical activation of the MAPK pathway by a selective inhibitor in cells bearing wild-type (WT) BRAF [29–31]. This feedback activation was significantly suppressed by DFG-out type multi-kinases inhibitors, but not by DFG-in type inhibitors. In addition, compared with type I inhibitors, type II

inhibitors have higher effectiveness [32]. Therefore, we aimed at discovering DFG-out type BRAF<sup>V600E</sup> and VEGFR-2 dual inhibitors.

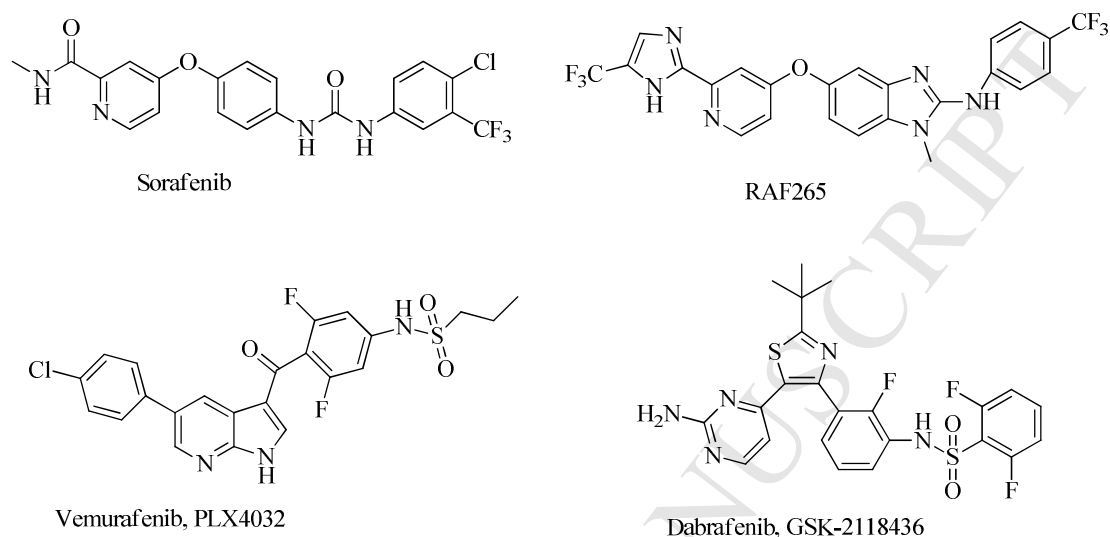
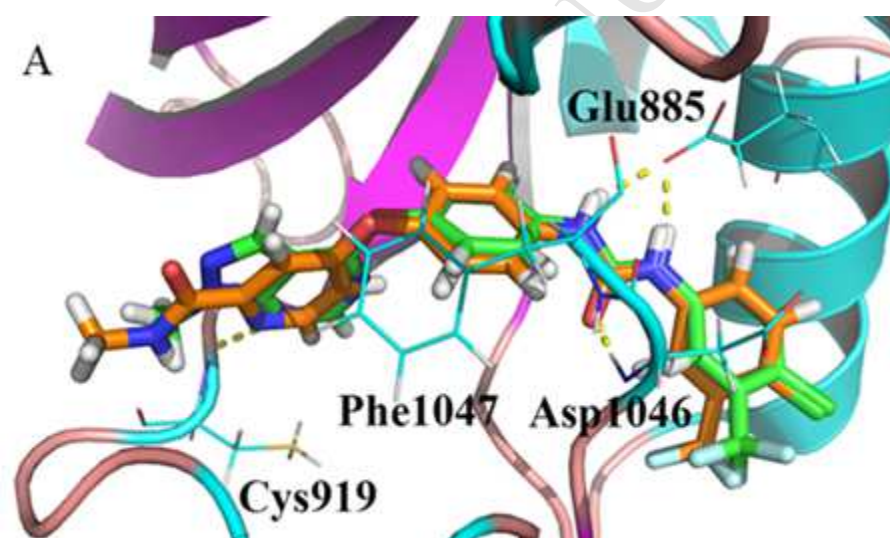


Fig. 1. Structure of BRAF<sup>V600E</sup>/VEGFR-2 dual inhibitors and selective BRAF<sup>V600E</sup> inhibitors.

At the time our program began, we have reported potent DFG-out type pan-RAF inhibitors and identified 1*H*-pyrazolo[3,4-*d*]pyrimidine **1** as an inhibitor of pan-RAF (BRAF<sup>V600E</sup> IC<sub>50</sub>, 23.6 nM; wild-type BRAF, 51.5 nM and C-RAF IC<sub>50</sub> = 8.5 nM) (Fig. 2) [33]. Compound **1** also showed effective anti-proliferative activities against RAF cell lines comparable to the efficacy of the positive control Sorafenib and significant suppression of downstream target MEK phosphorylation in BRAF<sup>V600E</sup> cell lines (A375 and HT-29) in a concentration-dependent manner. However, compound **1** showed poor inhibition activity on VEGFR-2 (IC<sub>50</sub> ≈ 1000 nM). These results imply that compound **1** could be exerting RAF inhibition on cancer cells rather than antiangiogenesis activity on vascular endothelial cells. On the basis of these results, we sought to increase the antiangiogenesis activity while retaining RAF kinase activity. As a means to understand the binding mode and generate a new chemotype for VEGFR-2 inhibition in addition to BRAF<sup>V600E</sup> inhibition, we docked **1** into the co-crystal structure of Sorafenib and VEGFR-2 to identify the key interactions between this molecule and the protein. Model of **1** in the active site of VEGFR-2 (PDB code: 3WZE [34]), which was

reported to be in the DFG-out inactive conformation, was constructed by using Glide in the XP mode [35-37] according to literature [38]. The best docking conformation based on the Glide score (G-score) was selected as the most probable binding conformation.

As shown in Fig. 2A, the model suggested that **1** overlapped well with the co-crystal ligand Sorafenib in the active site of VEGFR-2. The 1*H*-pyrazolo[3,4-*d*]pyrimidine ring in **1** occupied the ATP-binding pocket, and formed hydrogen bonds with Cys 919 in the hinge region of VEGFR-2. The diaryl urea portion extended into the large hydrophobic back pocket created by the rearrangement of the DFG motif, and the urea CO and NH moiety formed a hydrogen bond with the backbone-NH of Asp 1046 and side-chain carboxylate of Glu 855 in the DFG motif, respectively.



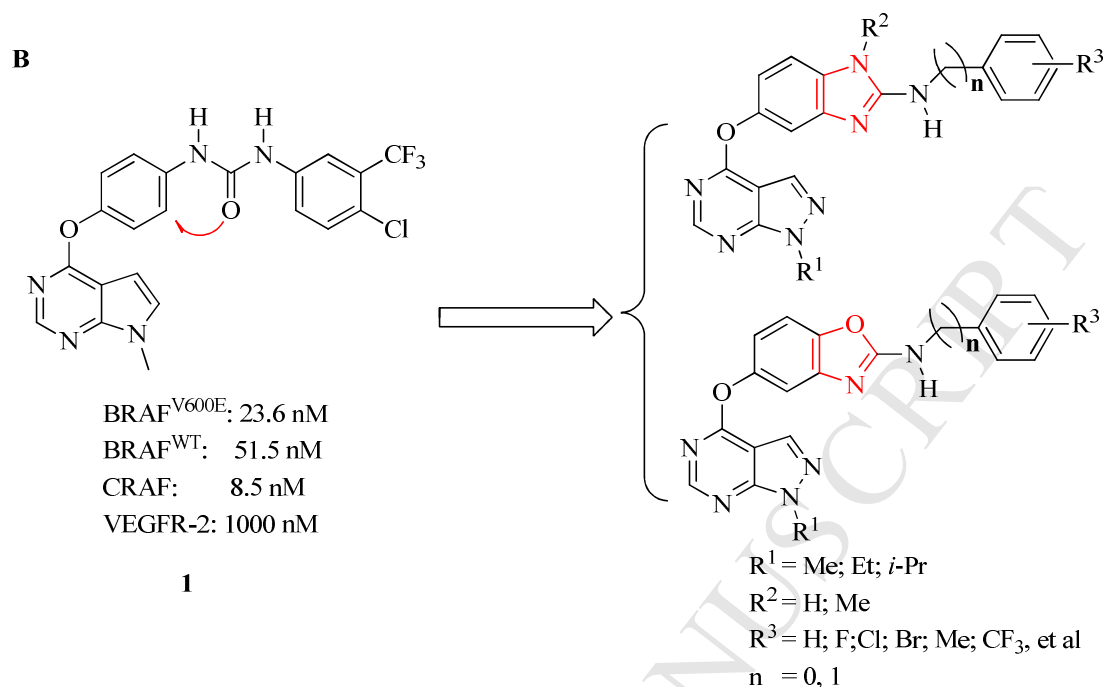


Fig. 2. (A) Model of compound **1** (green) overlaid with co-crystal structure of Sorafenib (orange) in the active site of VEGFR-2. (B) The design of BRAF<sup>V600E</sup> and VEGFR-2 dual inhibitors.

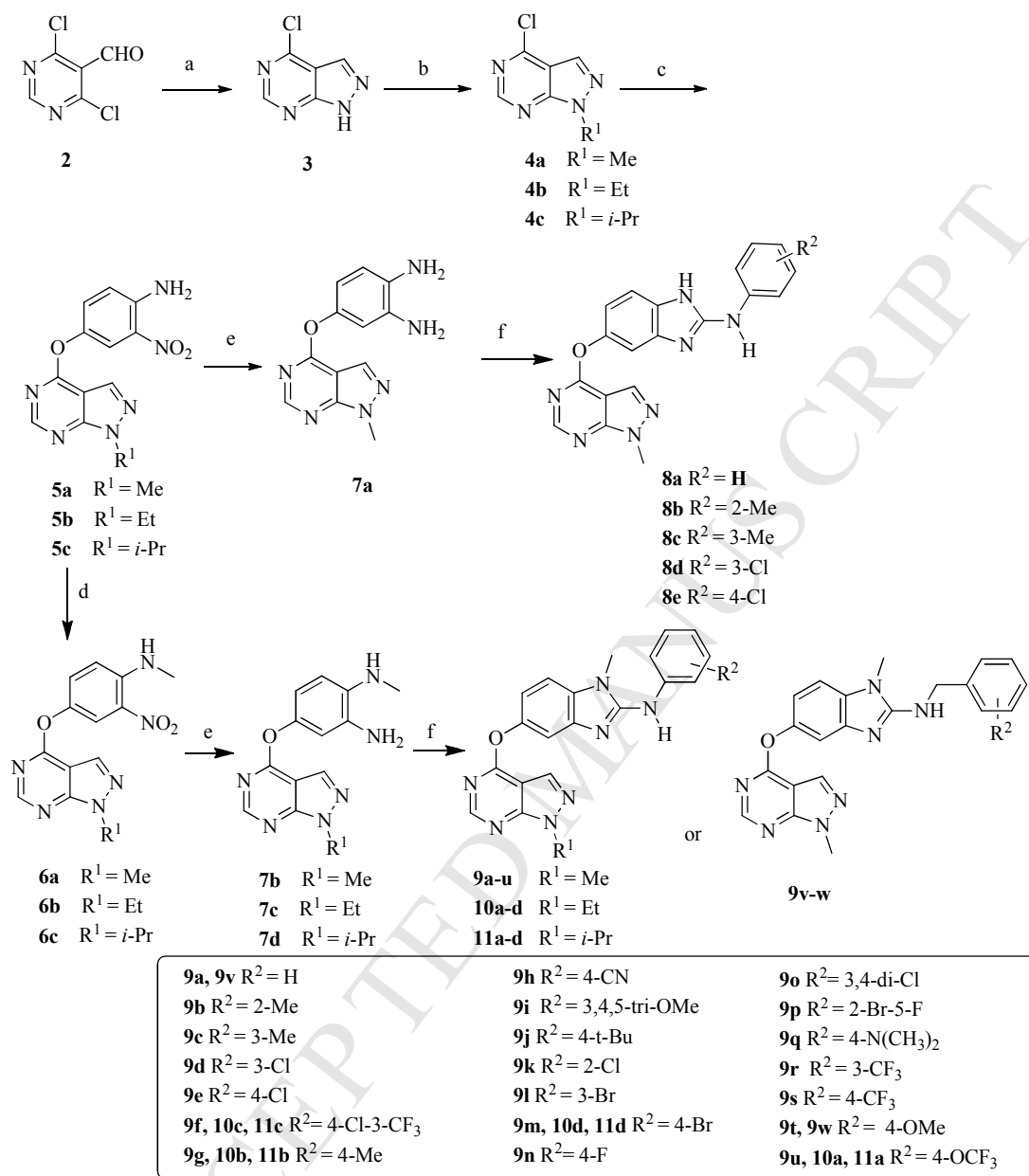
In order to improve inhibition activity of VEGFR-2 while retaining RAF kinase activity, on the basis of the above binding mode analysis, we proposed the cyclization of **1** to the corresponding 2-aminobenzimidazole to enhance conformational rigidity while maintaining the key hydrogen-bonding interactions (Fig. 2B). Reduced flexibility is expected to improve potency and physicochemical properties [39]. Guided by the structural information, we focus on the substitution on the terminal phenyl to investigate their effects on kinase inhibitory activities in this paper. In order to illustrate the effect of the 2-aminobenzimidazole ring on the inhibitory activity, 2-aminobenzoxazole compounds were also designed. Herein, we would like to report the synthesis and biological evaluation of these new compounds as BRAF<sup>V600E</sup>/VEGFR-2 dual inhibitors. The binding modes were disclosed by docking and molecular dynamics (MD) simulation, which verified our design strategy and displayed the structure-activity relationship.

## 2. Results and Discussion

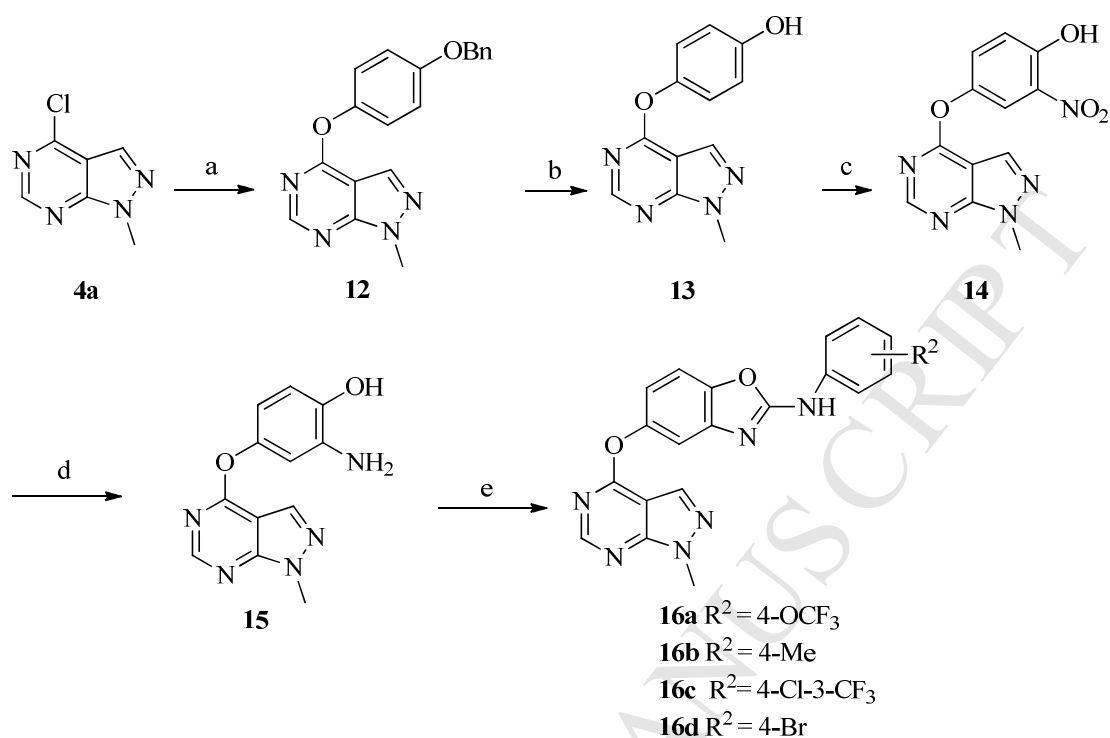
### 2.1 Chemistry

The 2-aminobenzimidazole compounds were easily constructed (Schemes 1). The intermediate **3** was synthesized with starting material 4,6-dichloropyrimidine-5-carbaldehyde (**2**) as described in our earlier research [33], which was under  $S_N2$  displacement reaction with iodoalkane to give **4**. The intermediate **5** was obtained by the  $S_NAr$  displacement reaction of **4** with 4-amino-3-nitrophenol. The intermediate **6** was achieved in a one-pot procedure by employing *in situ* protection of the amine with the trifluoroacetate group of **5**, followed by methylation with dimethyl sulfate using phase transfer catalysis [40]. Then subsequent reduction of the nitro group of intermediate **5** or **6** using 10% Pt/C and hydrazine hydrate afforded the desired phenylene-diamines **7**. Then phenylene-diamines **7** were treated with various isothiocyanates to afford thiourea intermediates, which were directly cyclized employing N,N-diisopropylcarbodiimide (DIC) to give the desired products (**8-11**) in moderate yields.

The synthetic strategy to prepare the 2-aminobenzoxazole compounds was illustrated in Schemes 2. Intermediate **3a** was treated with 4-benzyloxyphenol to yield biarylether **12**, which was deprotected using trifluoroacetic acid (TFA) to give corresponding phenol **13**. Regioselective nitration of phenol **13** using nitric acid afforded compound **14**. Reduction of the nitro group followed by addition of various isothiocyanates using the similar procedure as described for the preparation of 2-aminobenzimidazole compounds provided the target compounds **16**.



**Scheme 1.** Reagents and conditions: (a)  $\text{NH}_2\text{NH}_2 \cdot \text{H}_2\text{O}$ ,  $\text{NEt}_3$ ,  $\text{MeOH}$ ,  $-65^\circ\text{C}$ , 4 h; (b) iodoalkane,  $\text{Cs}_2\text{CO}_3$ ,  $\text{DMF}$ , rt, overnight; (c) 4-amino-3-nitrophenol,  $\text{Cs}_2\text{CO}_3$ ,  $\text{DMF}$ , rt, overnight; (d) (i) TFAA,  $\text{DCM}$ ,  $0^\circ\text{C}$ , 45 min; (ii)  $\text{Me}_2\text{SO}_4$ , hexadecyl trimethyl ammonium bromide (CTMAB), 50%  $\text{NaOH}$ , rt, overnight; (e) 10%  $\text{Pt/C}$ ,  $\text{NH}_2\text{NH}_2 \cdot \text{H}_2\text{O}$ ,  $\text{EtOH}$ , rt., 2-3 h; (f) (i) phenylisothiocyanate,  $\text{CH}_3\text{CN}$ , rt, 18 h; (ii) DIC,  $120^\circ\text{C}$ , 3-6 h.



**Scheme 2.** Reagents and conditions: (a) 4-(benzyloxy)phenol,  $\text{Cs}_2\text{CO}_3$ , DMF, rt, overnight; (b) TFA, 50 °C, overnight; (c) fuming  $\text{HNO}_3$ , AcOH, 30 °C, 2 h; (d) 10% Pt/C,  $\text{NH}_2\text{NH}_2 \cdot \text{H}_2\text{O}$ , EtOH, r.t., 1 h; (e) (i) phenylisothiocyanate,  $\text{CH}_3\text{CN}$ , rt, 18 h; (ii) DIC, 120 °C, 3-6 h.

## 2.2 Biological Activities and Discussion

### 2.2.1. Kinase Inhibitory Activity and SARs Study

The target compounds were evaluated for their inhibitory activities against  $\text{BRAF}^{\text{V600E}}$  and VEGFR-2 kinase using Sorafenib as positive control (Table 1). Based on the kinase activity evaluation, a preliminary structure-activity relationship (SAR) in this work was summarized in Fig 3. Unfortunately, closing the urea onto the internal phenyl led to **8a** with lower inhibitory activity for both the  $\text{BRAF}^{\text{V600E}}$  and VEGFR-2. Adding the substituent on the terminal phenyl of **8a** giving **8b-e** led to a slightly increased inhibitory activity for  $\text{BRAF}^{\text{V600E}}$  only. Guided by the molecular docking that NH of benzimidazole filled the small hydrophobic subpocket partially defined by the “gatekeeper” residue (Thr 529 for  $\text{BRAF}^{\text{V600E}}$ ), introduction of a methyl on the 2-aminobenzimidazole NH was explored giving **9a-e**. Compared to the unmethylated analogues **8a-e**, **9a-e** exhibited better inhibitory

activities against BRAF<sup>V600E</sup> and VEGFR-2. In addition, the replacement of NH of 2-amino benzimidazole with O gave compound 2-aminobenzoxazole compounds **16**, which displayed decreased inhibitory activities against BRAF<sup>V600E</sup> and VEGFR-2, particularly for VEGFR-2. Apparently, the N-Me of benzimidazole turned out to be optimal for BRAF<sup>V600E</sup> and VEGFR-2 inhibition.

Then, systematic evaluation of various substituents at the terminal phenyl was conducted. Almost all compounds with substitution at the terminal phenyl can improve the inhibitory activity compared to unsubstituted compound **9a**, indicating substitution on the aryl ring was essential for potent BRAF<sup>V600E</sup> and VEGFR-2 inhibition. It also indicated the importance of the hydrophobic interaction between the inhibitor and the hydrophobic amino acid residues of the back pocket created by the rearrangement of the DFG motif. Compound **9f** with the same substitution on the terminal phenyl with Sorafenib and **1** displayed potent inhibition of VEGFR-2, while the inhibition of BRAF<sup>V600E</sup> decreased significantly. In general, introduction of substituents on the 4-position of the terminal phenyl led to higher inhibitory activities for BRAF<sup>V600E</sup> and VEGFR-2 than substitution on the 2- and 3-positions. For example, compound **9g** exhibited higher inhibition against both the BRAF<sup>V600E</sup> and VEGFR-2 than **9b** and **9c**. A variety of substituents at the *para*-position, including both electron-donating and electron-withdrawing groups were tolerated, which suggested that the electronic interaction of the substituent had little effect on the kinase inhibitory activities. For example, introduction of the electron-donating group methyl and methoxy in compounds **9g** and **9t** increase the inhibitory activities, and substitution with electron-withdrawing groups such as Cl, Br, and CF<sub>3</sub> on the phenyl ring also led to enhancement of kinase inhibitory activities (**9e**, **9m** and **9s**). Particularly, compound **9m** with a 4-bromo substituent exhibited kinase inhibitory activity against VEGFR-2 that was about 30-fold better than **1**, while with slightly weaker potency for BRAF<sup>V600E</sup> compared to that of compound **1**. The necessity of the terminal aryl in retaining high potency was also evidenced by the fact that substituting with aliphatic residue, such as benzyl (**9v** and **9w**), led to the decrease of inhibitory activities. This SAR was consistent with the molecular modeling that the terminal phenyl group in **1** projected into the large hydrophobic pocket created by the rearrangement



<b>9e</b>	NMe	Me	4-Cl	91.1(105.6) <sup>b</sup>	105.6 (49.8) <sup>b</sup>	>100	73.56	84.32
<b>9f</b>	NMe	Me	4-Cl-3-CF <sub>3</sub>	55.1	97.7 (134.5) <sup>b</sup>	1.99	14.38	13.47
<b>9g</b>	NMe	Me	4-Me	90.1 (85.2) <sup>b</sup>	96.6 (17.1) <sup>b</sup>	25.36	6.13	15.71
<b>9h</b>	NMe	Me	4-CN	70.7	88.7	>100	>100	62.7
<b>9i</b>	NMe	Me	3,4,5-tri-OCH <sub>3</sub>	26.8	40.7	>100	>100	>100
<b>9j</b>	NMe	Me	4- <i>t</i> -Bu	50.8	84.2 (140) <sup>b</sup>	1.23	75.41	53.51
<b>9k</b>	NMe	Me	2-Cl	65.4	84.2	>100	80.36	78.62
<b>9l</b>	NMe	Me	3-Br	65.7	73.7	82.18	64.29	74.24
<b>9m</b>	NMe	Me	4-Br	102.3 (40.9) <sup>b</sup>	108.9 (29.9) <sup>b</sup>	30.25	>100	7.89
<b>9n</b>	NMe	Me	4-F	85.6 (407.2) <sup>b</sup>	94.0 (41.7) <sup>b</sup>	68.42	79.14	12.81
<b>9o</b>	NMe	Me	3,4-di-Cl	68.1 (487.8) <sup>b</sup>	82.2 (120.4) <sup>b</sup>	66.68	81.20	>100
<b>9p</b>	NMe	Me	2-Br-5-F	51.4	48.6	>100	>100	>100
<b>9q</b>	NMe	Me	4-N(CH <sub>3</sub> ) <sub>2</sub>	67.2	94.5 (111.5) <sup>b</sup>	5.19	65.44	>100
<b>9r</b>	NMe	Me	3-CF <sub>3</sub>	80.5 (476.3) <sup>b</sup>	88.1 (150.2) <sup>b</sup>	10.08	>100	29.23
<b>9s</b>	NMe	Me	4-CF <sub>3</sub>	74.4 (215.6) <sup>b</sup>	97.4 (63.2) <sup>b</sup>	4.11	63.21	12.56
<b>9t</b>	NMe	Me	4-OCH <sub>3</sub>	79.6	93.6 (73.4) <sup>b</sup>	13.72	>100	90.89
<b>9u</b>	NMe	Me	4-OCF <sub>3</sub>	83.1 (171.5) <sup>b</sup>	96.4 (77.9) <sup>b</sup>	1.74	6.92	5.89
<b>9v</b>	NMe	Me	H	6.66	9.12	>100	32.48	>100
<b>9w</b>	NMe	Me	4-OCH <sub>3</sub>	53.6	102.3 (424) <sup>b</sup>	9.31	>100	20.36
<b>10a</b>	NMe	Et	4-OCF <sub>3</sub>	19.6	59.6	8.52	12.25	54.42
<b>10b</b>	NMe	Et	4-Me	68.0	85.5	4.82	6.71	5.25
<b>10c</b>	NMe	Et	4-Cl-3-CF <sub>3</sub>	10.9	44.7	5.19	8.51	8.17
<b>10d</b>	NMe	Et	4-Br	69.4	81.1	7.12	8.01	10.15
<b>11a</b>	NMe	<i>i</i> -Pr	4-OCF <sub>3</sub>	13.2	15.1	7.46	9.51	5.96
<b>11b</b>	NMe	<i>i</i> -Pr	4-Me	36.0	35.2	33.06	13.89	29.58
<b>11c</b>	NMe	<i>i</i> -Pr	4-Cl-3-CF <sub>3</sub>	7.5	6.1	15.71	36.85	37.64
<b>11d</b>	NMe	<i>i</i> -Pr	4-Br	33.3	38.5	12.82	9.01	15.86
<b>16a</b>	O	Me	4-OCF <sub>3</sub>	56.1	22.3	>100	>100	61.62
<b>16b</b>	O	Me	4-Me	81.6	53.1	44.92	28.25	35.37
<b>16c</b>	O	Me	4-Cl-3-CF <sub>3</sub>	20.0	15.6	44.21	34.02	>100
<b>16d</b>	O	Me	4-Br	60.1	18.9	>100	41.07	17.19
	Sorafenib			94.5 (52.3) <sup>b</sup>	94.3 (17.6) <sup>b</sup>	8.33	2.58	2.69

<sup>a</sup> Values indicate the kinase inhibition % at 1 $\mu$ M, which are the average of two independent experiments.

<sup>b</sup> Values in the parentheses indicate IC<sub>50</sub> ( nM ), which are the average of two independent experiments.

<sup>c</sup> IC<sub>50</sub> values are presented as mean values of at least three independent experiments.

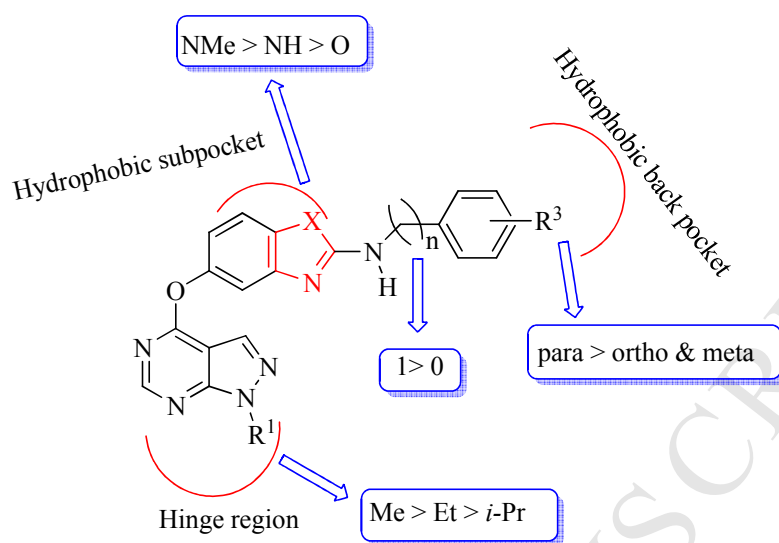


Fig. 3 Preliminary structure-activity relationships

### 2.2.2 *In vitro* Anti-proliferative Activities

The cell growth inhibitory activities of target compounds were evaluated against human cancer A375 and HT-29 cell lines highly expressing the BRAF<sup>V600E</sup> protein as well as the HUVEC cell line highly expressing the VEGFR-2 protein by the standard MTT assay, with Sorafenib as the positive control. The *anti*-proliferative activities were reported in Table 1. It can be noted that most of the target compounds displayed moderate to high potency against A375, HT-29 and HUVEC cell, some of the compounds showed parallel anti-proliferative activities as Sorafenib. For example, compounds **9f**, **9j**, **9q**, **9s**, **9u**, **9w**, **10a-d**, **11a** and compounds **9g**, **9u**, **10b-d**, **11a**, **11d** displayed significant potency against BRAF<sup>V600E</sup>-expressing A375 and H-29 with IC<sub>50</sub> values of 1.23-9.31 μM and 6.13-9.51 μM, respectively, which turned out to be similar to that of Sorafenib (8.33 and 2.58 μM for A375 and HUVEC, respectively). In addition, compounds **9m**, **9u**, **10b-c** and **11a** displayed significant potency against VEGFR-2- expressing HUVEC with IC<sub>50</sub> values of 5.25-8.17 μM, which was similar to that of Sorafenib (2.69 μM). Nevertheless, the cellular responses of some synthesized compounds were not consistent with the enzymatic assays absolutely. For example, although **9e**, **9g**, and **9m** exhibited good enzyme potencies against BRAF<sup>V600E</sup> and VEGFR-2, they showed moderate cell growth inhibitory activities compared to Sorafenib. This discrepancy between biochemical and

cell potency could be explained that in the biochemical assay purified kinase domains of BRAF<sup>V600E</sup> and VEGFR-2 were being tested compared to the cellular assay in which kinases exist as a complex with chaperons, cytoskeleton, phosphatases and kinases [41]. In contrast, compounds **10a-d** and **11a** with poor kinase inhibitory activities showed significant cell growth inhibitory activities, which may be related to the complicated mechanism of tumor cell survival or proliferation that is regulated by several different factors [42], or through alternate mechanism but not by targeting BRAF<sup>V600E</sup> or VEGFR-2 [43-44].

### 2.2.3 Kinase Inhibitory Profile of Compound **9u**

Compound **9u** exhibited high inhibitory activity against BRAF<sup>V600E</sup> (IC<sub>50</sub> = 0.171 μM) and VEGFR-2 (IC<sub>50</sub> = 0.779 μM), and effective anti-proliferative potencies against three cell lines (A375, HT-29, and HUVEC), which were comparable to the efficacy of Sorafenib. Therefore, we selected **9u** for further investigation. The kinase selectivity profile of **9u** was assessed over 17 different protein kinases (Table 2). As shown in Table 2, compound **9u** had moderate inhibitory activity against CRAF (inhibition % = 87.6), almost poor or no significant inhibitory activity against wild-type (WT) BRAF and 15 other tested protein kinases even at concentration of 1000 nM, which revealed that compound **9u** had a very good selectivity profile and was a BRAF<sup>V600E</sup>/VEGFR-2 kinases dual inhibitor.

Table 2. Kinase selectivity profile of compound **9u**

Kinase tested	Inhibition % at 1 μM <sup>a</sup>	Kinase tested	Inhibition % at 1 μM <sup>a</sup>
BRAF (WT)	13.7	SRC	14.0
CRAF (RAF-1)	87.6	AURKB (Aurora B)	-11.6
PDGFRA (PDGFR α)	21.9	LCK	5.9
PDGFRB (PDGFR β)	35.6	ALK	-11.7
FGFR3	-4.9	MET (c-Met)	24.9
KIT	25.4	PTK6 (Brk)	-6.7
CSF1R (FMS)	40.5	FGR	-6.9
FLT1 (VEGFR-1)	54.7	SRMS	7.1
FLT4 (VEGFR-3)	52.0		

<sup>a</sup> Values are the average of two independent experiments.

#### 2.2.4 Flow Cytometric Analysis of Cell-cycle Arrest

To study the effect of these target compounds on cells cycle progression, flow-activated cell sorting analysis was performed. The most promising compound **9u** was tested against A375 and HUVEC cell lines at given concentrations, respectively. Interestingly, very similar changes in cell cycle distribution were observed. A375 and HUVEC cell lines were arrested by compound **9u** in G<sub>0</sub>/G<sub>1</sub> phase with a concentration-dependent effect compared to untreated control cells. As shown in Figure 4-5 and Table 3-4, the 'G<sub>0</sub>/G<sub>1</sub>' peak in A375 cell line significantly increased from 62.83% to 70.33% (0.87 μM), 75.34% (1.74 μM), 84.97% (3.48 μM), and the 'G<sub>0</sub>/G<sub>1</sub>' peak of HUVEC significantly increased from 53.18% to 69.74% (2.95 μM), 77.70% (5.89 μM), 83.26% (11.78 μM) after 48 h of incubation with the compound **9u**.

Table 3. Effect of compound **9u** on cell cycle distribution in A375 cell line.

Concentration	Sub-G <sub>1</sub> (%)	G <sub>0</sub> /G <sub>1</sub> (%)	S (%)	G <sub>2</sub> /M (%)
0	2.32	62.83	14.8	19.75
0.87 μmol/L	3.21	70.33	10.78	14.92
1.74 μmol/L	4.36	75.34	9.97	10.09
3.48 μmol/L	3.05	84.97	7.02	4.38

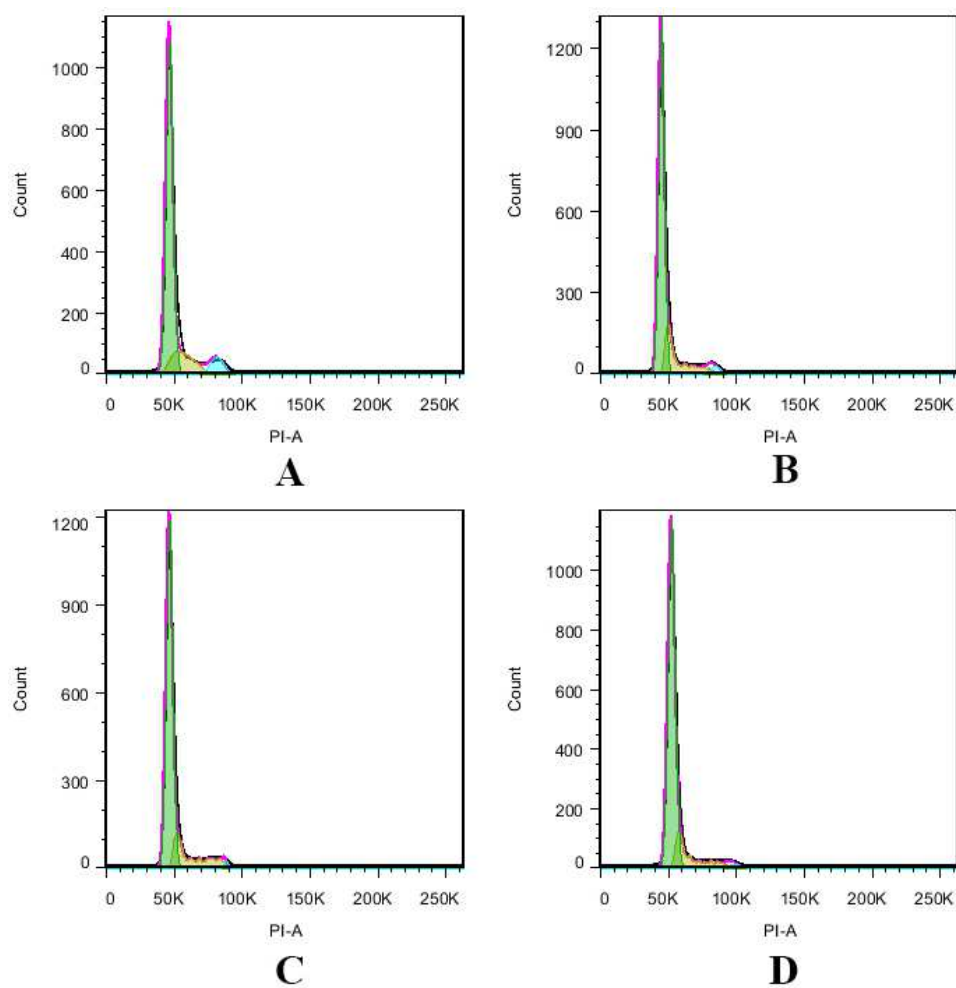


Fig. 4. Flow cytometric analysis of cell cycle distribution in A375 cell line treated with **9u** for 48 h. (A) Control; (B) 0.87  $\mu\text{mol/L}$  ( $1/2 \text{ IC}_{50}$ ); (C) 1.74  $\mu\text{mol/L}$  ( $1 \text{ IC}_{50}$ ); (D) 3.48  $\mu\text{mol/L}$  ( $2 \text{ IC}_{50}$ ).

Table 4. Effect of compound **9u** on cell cycle distribution in HUVEC cell line.

Concentration	Sub-G <sub>1</sub> (%)	G <sub>0</sub> /G <sub>1</sub> (%)	S (%)	G <sub>2</sub> /M (%)
0	1.36	53.18	24.3	20.11
2.95 $\mu\text{mol/L}$	2.68	69.74	12.54	14.92
5.89 $\mu\text{mol/L}$	1.94	77.70	9.24	10.34
11.78 $\mu\text{mol/L}$	2.63	83.26	9.89	3.85

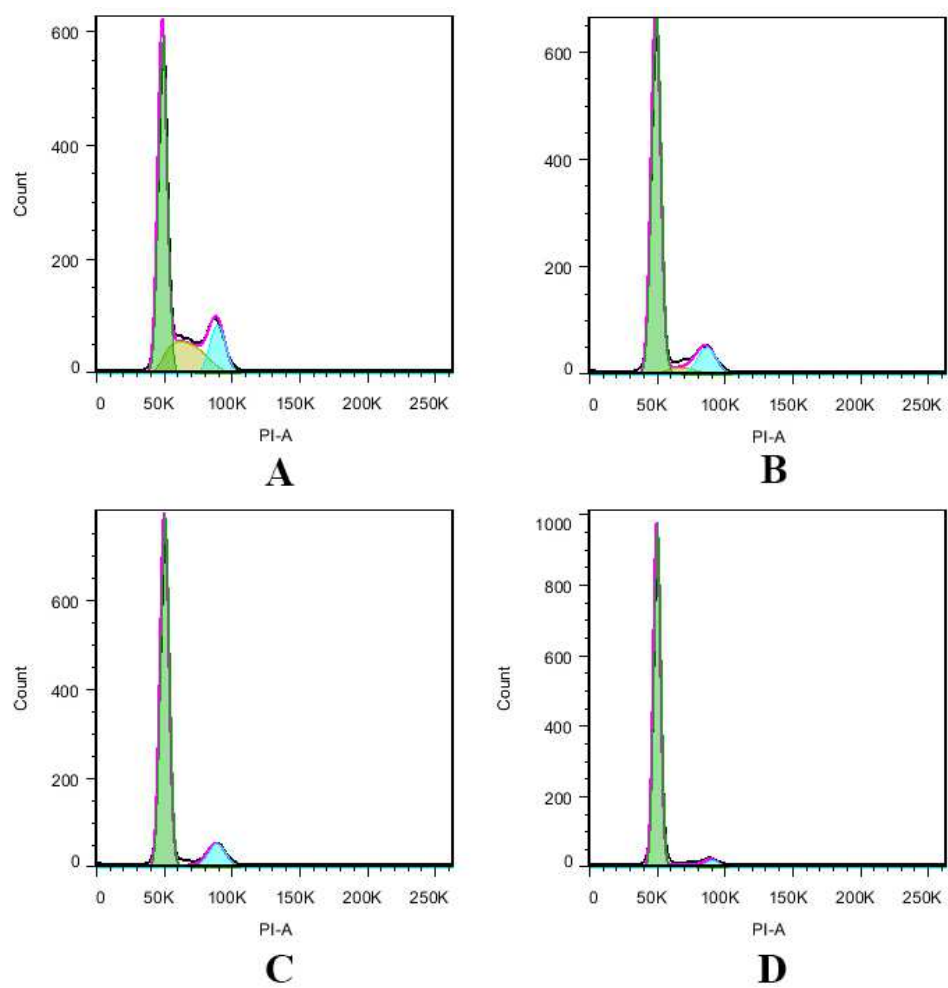


Fig. 5. Flow cytometric analysis of cell cycle distribution in HUVEC cell line treated with **9u** for 48 h. (A) Control; (B) 2.95  $\mu\text{mol/L}$  ( $1/2 \text{ IC}_{50}$ ); (C) 5.89  $\mu\text{mol/L}$  ( $1 \text{ IC}_{50}$ ); (D) 11.78  $\mu\text{mol/L}$  ( $2 \text{ IC}_{50}$ ).

## 2.4 Molecular Modeling

In order to understand the interaction between the synthesized compounds and kinases, docking experiments of the representative compounds **8a**, **9u**, **9w**, **10a**, **11a** and **16a** into the active site of BRAF<sup>V600E</sup> and VEGFR-2 (PDB code: 1UWJ [45] and 3WZE [34], respectively), which were reported to be in the DFG-out inactive conformation of kinase, was constructed using Glide (Grid-based Ligand Docking with Energetics) in Extra-Precision (XP) mode [35-37]. The docking results indicated that all the representative compounds could dock into the active site of BRAF<sup>V600E</sup> and KDR (Figure 6) and adopt a similar binding mode with the compound **1** and Sorafenib except for compound **9w** with benzyl group on the terminal (Fig. S1 of supporting information). The compound **9u** was taken as an example to illustrate the binding modes. The *1H*-pyrazolo[3,4-*d*]pyrimidine moiety inserted into the deep cleft of ATP-binding site and formed hydrogen-bond with the backbone-NH of Cys532 and Cys919 from hinge region of BRAF<sup>V600E</sup> and VEGFR-2, respectively, and the 2-aminobenzimidazole formed hydrogen-bond interactions with the DFG motif of BRAF<sup>V600E</sup> and VEGFR-2, respectively. The terminal 4-trifluoromethoxyphenyl portion extended into the large hydrophobic back pocket created by the rearrangement of the DFG motif, which was consistent with the structure-activity relationship (SAR) that the introduction of hydrophobic groups was beneficial for potency. The N-Me on the 2-aminobenzimidazole filled the small hydrophobic subpocket partially defined by the “gatekeeper” residue (Thr 529 for BRAF<sup>V600E</sup>), which can partially explain the decreased inhibitory activities of compounds **8a-e** with unmethylated benzimidazole scaffold and compounds **16a-d** with 2-aminobenzoxazole scaffold. The introduction of larger groups in the N1 position of *1H*-pyrazolo[3,4-*d*]pyrimidine led to deterioration of the potency because of the steric hindrance effect with the hinge region. The compound **9w** adopted a distinct binding mode that cannot form H-bond with the backbone-NH of Cys532 from hinge region of BRAF<sup>V600E</sup>, which gave explanation for the decreased activity for BRAF<sup>V600E</sup> (Fig. S1 of supporting information).

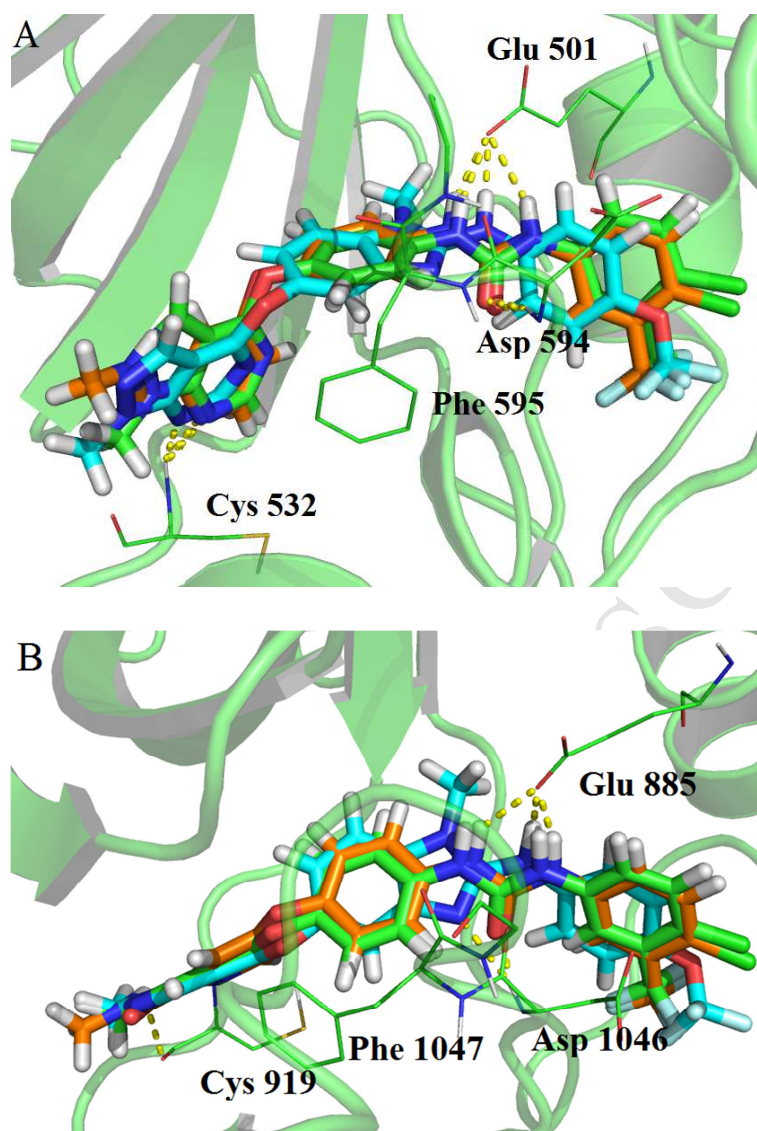


Fig. 6. (A) The docked binding modes of compound **1** (green) and **9u** (cyan) overlaid with co-crystal structure of Sorafenib (orange) in the active site of BRAF<sup>V600E</sup> (A) and VEGFR-2 (B). (BRAF<sup>V600E</sup> and VEGFR-2 in colored cartoon, ligand in stick model and the key residues in line model. Yellow dots represent hydrogen bonds.)

The best docking conformations of the potent compound **9u** based on the Glide score (G-score) were selected as the most probable binding conformation, which were subjected to molecular dynamics (MD) simulation to explore in depth the binding poses. MD simulations were then carried out in explicit aqueous solution for 50 ns. For comparison, MD simulations of positive control Sorafenib in complex with BRAF<sup>V600E</sup> and VEGFR-2 were also performed. The stability of four systems under simulation was evaluated by the root-mean-square deviation (RMSD) of the backbone atoms relate to

the starting structures (Fig. 7). As can be seen in the plot, all systems were stable during the 50-ns MD simulation. Moreover, we compared the representative snapshots of each complex taken from the last 10 ns MD trajectories with the initial structure (Fig. 8). As illustrated in Figure 8, the binding modes of **9u** from MD were nearly the same as the docked structures.

The hydrogen bond plays an important role in the binding of inhibitor with kinase. As we expected, the *1H*-pyrazolo[3,4-*d*]pyrimidine moiety can form H-bond with the backbone-NH of Cys532 and Cys919 from hinge region of BRAF<sup>V600E</sup> and VEGFR-2 with very high hydrogen-bond occupancies of 91.76 and 91.04 %, respectively (Table 5). Unlike the compound **9u**, Sorafenib could form a pair of H-bonds with Cys532 and Cys919 of BRAF<sup>V600E</sup> and VEGFR-2, respectively. In comparison to Sorafenib, compound **9u** formed moderate hydrogen bond interactions with Asp594 and Asp1046 of BRAF<sup>V600E</sup> and VEGFR-2, respectively, which could partially explain that compound **9u** displayed lower inhibitory activity than Sorafenib. Besides, both compound **9u** and Sorafenib form hydrogen bond interactions with side-chain carboxylate of Glu501 and Glu885 from the DFG motif of BRAF<sup>V600E</sup> and VEGFR-2 with very high hydrogen-bond occupancies, respectively.

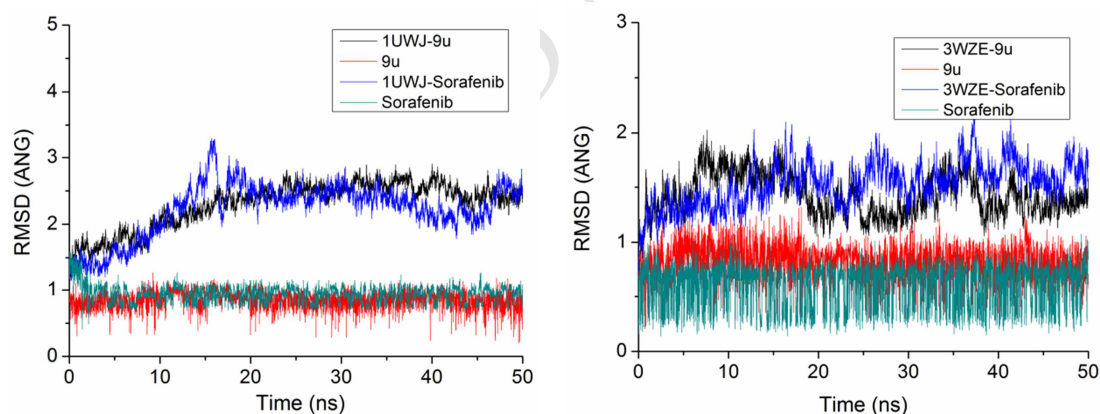


Fig. 7. Root-mean-square deviations (RMSDs) of backbone atoms (C, C $\alpha$  and N) of protein, and the heavy atoms of the ligand for the simulated systems.

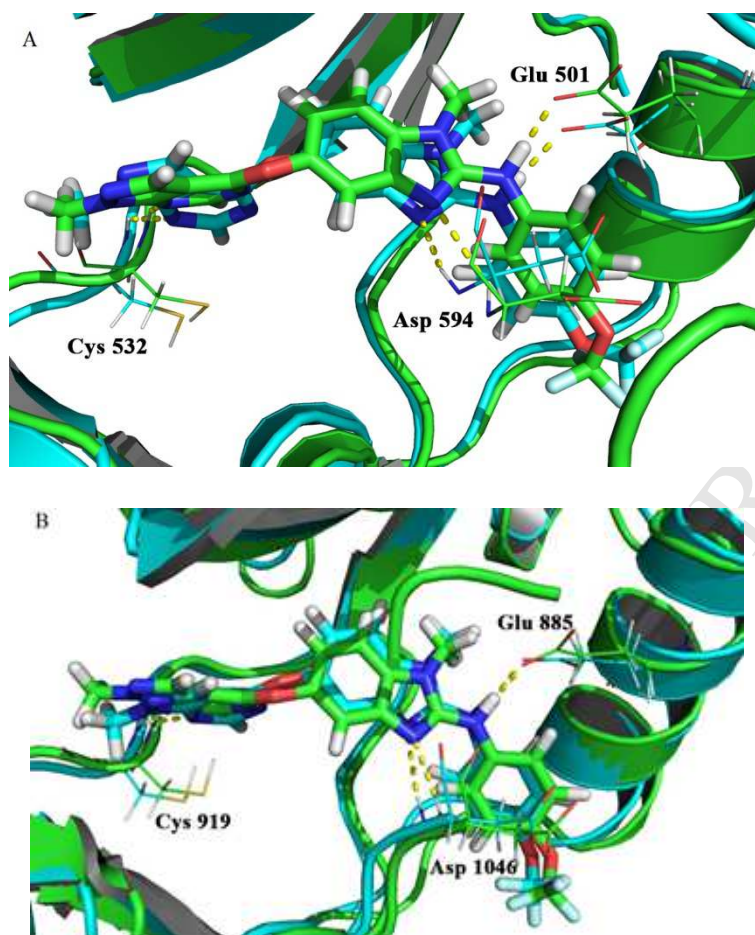


Fig.8. Structural comparison between docked (green) and molecular dynamics simulated representative snapshots (cyan) of **9u** in the active site of BRAF<sup>V600E</sup> (A) and VEGFR-2 (B). (BRAF<sup>V600E</sup> and VEGFR-2 in colored cartoon, ligand in stick model and the key residues in line model. Yellow dots represent hydrogen bonds.)

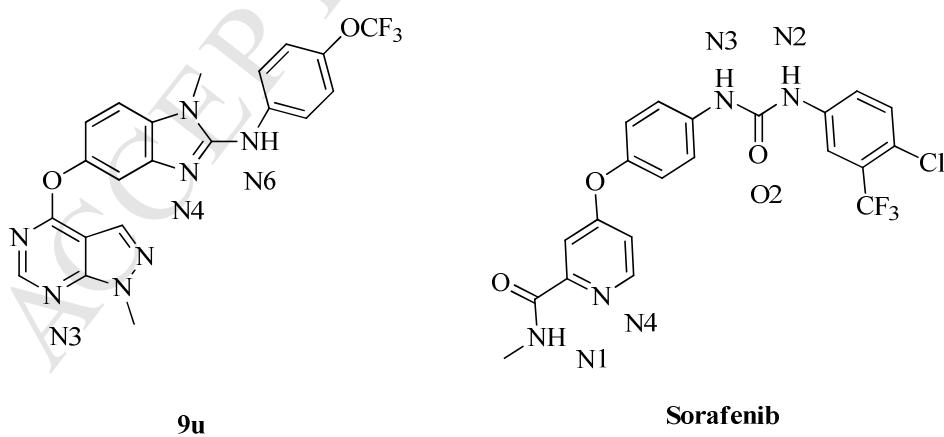


Table 5. Main hydrogen-bond interactions between inhibitors and BRAF<sup>V600E</sup> and VEGFR-2.

	BRAF <sup>V600E</sup>			VEGFR-2		
	Acceptor	Donor	Occupancy (%) <sup>a</sup>	Acceptor	Donor	Occupancy (%) <sup>a</sup>
<b>9u</b>	Lig @N3	Cys532@NH	91.76	Lig @N3	Cys919@NH	91.04
	Lig @N4	Asp594@NH	66.12	Lig @N4	Asp1046@NH	57.11
	Glu501@OE1	Lig @N6H	59.05	Glu885 @OE1	Lig @N6H	56.69
	Glu501@OE2	Lig @N6H	39.34	Glu885 @OE2	Lig @N6H	37.63
Sorafenib	Lig @O2	Asp594@NH	99.07	Lig @O2	Asp1046@NH	96.83
	Glu501@OE1	Lig @N2H	63.16	Glu885 @OE1	Lig @N2H	54.34
	Glu501@OE2	Lig @N3H	62.73	Glu885 @OE2	Lig @N3H	53.52
	Glu501@OE1	Lig @N3H	37.07	Glu885 @OE1	Lig @N3H	45.69
	Glu501@OE2	Lig @N2H	36.90	Glu885 @OE2	Lig @N2H	46.69
	Lig @N4	Cys532@NH	27.88	Lig @N4	Cys919@NH	79.28
	Cys532@O	Lig @N1H	42.63	Cys919@O	Lig @N1H	61.10

<sup>a</sup> Occupancy is in unit of percentage of the investigated time period.

The binding-free energies were calculated by using MM-PBSA (molecular mechanics Poisson–Boltzmann surface area) and MM-GBSA (molecular mechanics Generalized-Born surface area) programs in AMBER (Table 6). As can be seen, MM-PBSA and MM-GBSA calculations verified that **9u** showed decreased potency ligand compared to that of Sorafenib, which was in good agreement with the experimental data. According to the energy individual components of the binding-free energies, the favorable contributors to ligand binding were van der Waals (vdW) terms, electrostatic and nonpolar solvation energies, whereas polar solvation and entropy terms oppose binding. The favorable electrostatic interactions were counteracted by the unfavorable electrostatics of desolvation upon binding. Consequently, the total electrostatic interaction contributions were unfavorable to binding in all systems.

Table 6. Binding-free energies for **9u** and Sorafenib in complex with BRAF<sup>V600E</sup> and VEGFR-2 obtained by MM-PBSA and MM-GBSA (kcal/mol)<sup>a</sup>

	<b>9u</b>		Sorafenib	
	BRAF <sup>V600E</sup>	VEGFR-2	BRAF <sup>V600E</sup>	VEGFR-2
$\Delta E_{\text{vdW}}$	-62.51 (2.72)	-68.80 (2.55)	- 57.10 (2.75)	-59.92 (2.63)
$\Delta E_{\text{ele}}$	-25.57 (3.48)	-21.35 (2.79)	- 35.27 (3.72)	-36.33 (3.35)
$\Delta E_{\text{MM}}$	-88.08 (3.82)	- 90.15 (3.26)	- 92.37 (4.11)	- 96.25 (3.68)
$\Delta G_{\text{ele,sol}}(\text{GB})$	42.20 (2.34)	39.21 (1.76)	45.71 (2.66)	44.67 (2.18)
$\Delta G_{\text{np,sol}}(\text{GB})$	-7.51 (0.17)	- 7.77 (0.15)	- 7.78 (0.18)	- 7.93 (0.17)

$\Delta G_{\text{sol}}$ (GB)	34.69 (2.24)	31.45 (1.80)	37.93 (2.63)	36.74 (2.20)
$\Delta G_{\text{ele,sol}}$ (PB)	47.84 (2.51)	43.77 (2.14)	49.93 (3.01)	47.64 (2.54)
$\Delta G_{\text{np,sol}}$ (PB)	-4.52 (0.09)	-4.39 (0.08)	-4.57 (0.09)	-4.55 (0.08)
$\Delta G_{\text{sol}}$ (PB)	43.32 (2.51)	39.38 (2.12)	45.36 (2.99)	43.08 (2.52)
$\Delta H_{\text{pred}}$ (GB)	-53.38 (3.01)	-58.70 (2.83)	-54.44 (2.98)	-59.52 (3.10)
$\Delta H_{\text{pred}}$ (PB)	-47.75 (3.25)	-50.77 (3.10)	-47.01 (3.60)	-53.17 (3.24)
T $\Delta S$	-27.73 (5.66)	-27.46 (2.64)	-25.39 (6.27)	-25.20 (2.31)
$\Delta G_{\text{pred}}$ (GB)	-25.65	-31.24	-29.05	-34.32
$\Delta G_{\text{pred}}$ (PB)	-20.02	-23.31	-21.62	-27.97

<sup>a</sup>  $\Delta G_{\text{pred}}$ : the calculated binding-free energy by MM-PBSA and MM-GBSA method

$$\Delta H_{\text{pred}} = \Delta G_{\text{ele}} + \Delta G_{\text{vdW}} + \Delta G_{\text{np,sol}} + \Delta G_{\text{ele,sol}}$$

$$\Delta G_{\text{pred}} = \Delta G_{\text{ele}} + \Delta G_{\text{vdW}} + \Delta G_{\text{np,sol}} + \Delta G_{\text{ele,sol}} - T\Delta S$$

### 3. Conclusion

In conclusion, a series of 1*H*-pyrazolo[3,4-*d*]pyrimidine derivatives were designed, synthesized and evaluated for their BRAF<sup>V600E</sup> and VEGFR-2 inhibitory activity as well as their anti-proliferative activity. The preliminary investigation showed most of the synthesized 1*H*-pyrazolo[3,4-*d*]pyrimidine compounds displayed moderate to high potent activity in both enzymatic and cellular proliferation assays. Among these compounds, **9e**, **9g**, **9m** and **9u** showed remarkably high inhibitory activities against both BRAF<sup>V600E</sup> and VEGFR-2 kinase comparable to positive control Sorafenib. Particularly, compound **9u** also showed potent *anti*-proliferative activity against BRAF<sup>V600E</sup>-expressing A375 and H-29 as well as VEGFR-2-expressing HUVEC, which was also comparable to Sorafenib. Furthermore, **9u** showed almost poor or no significant inhibitory activity against wild-type BRAF and 15 other tested protein kinases, implying a very good selectivity profile. Flow cytometric analysis showed that compound **9u** mainly arrested the A375 and HUVEC cell lines in the G<sub>0</sub>/G<sub>1</sub> stage with a concentration-dependent effect. In addition, the molecular docking and MD simulations suggested a similar binding pattern with Sorafenib at the ATP-binding sites of BRAF<sup>V600E</sup> and VEGFR-2. Taken together, these results indicated that compound **9u** may serve as novel lead compounds in research on more effective BRAF<sup>V600E</sup> and VEGFR-2 dual inhibitors.

### 4. Experimental

#### 4.1. Chemistry

All starting materials, reagents, and solvents were purchased from commercial vendors and were used without further purification. All oxygen-sensitive or moisture-sensitive reactions were run under nitrogen atmosphere. Yields were not optimized. Reactions were monitored by thin-layer chromatography (TLC) on silica gel plates at 254 nm under an ultraviolet (UV) light. Flash column chromatography separations were performed on normal phase silica gel (200-300 mesh, Merck) or reverse phase silica gel by using Yamazen AI-580 flash chromatography (Yamazen Co., Osaka, Japan) with UV detection at 254 nm.  $^1\text{H}$  and  $^{13}\text{C}$  NMR spectra were recorded on a BRUKER AVIII 400 MHz and 101 MHz spectrometer with tetramethylsilane (TMS) as the internal standard, the values of the chemical shifts ( $\delta$ ) are given in ppm, and coupling constants ( $J$ ) are given in Hz. Mass spectra (ESI-MS) were performed on WATERS ZQ4000 (Waters Co., Milford, MA, USA). High resolution mass spectra (HRMS) were recorded on a Thermo Fisher Scientific Orbitrap Fusion Tribrid (Q-OT-qIT) mass spectrometer (Thermo Fisher Scientific, Bremen, German). FT-IR spectra were recorded on a Thermo Scientific Nicolet 6700 spectrometer. Melting points were determined using an X-4 melting-point apparatus with microscope (Gongyi Yuhua Instrument Co., Ltd., Henan, China) and were uncorrected.

#### 4.1.1. 4-chloro-1H-pyrazolo[3,4-d]pyrimidine (**3**)

To the solution of 4,6-dichloropyrimidine-5-carbaldehyde **2** (1.0 g, 5.6 mmol) in methanol (20 mL) at  $-65\text{ }^\circ\text{C}$ , triethylamine (0.97 mL) was added. A solution of hydrazine monohydrate (0.274 mL 1.0 eq.) in methanol (10 mL) was slowly dripped into above stirred solution by using a constant-pressure dropping funnel. The mixture was allowed to warm to room temperature and stirred for 2–3 h. The reaction mixture was concentrated *in vacuo* and crude product was diluted with water (20 mL), and extracted with EtOAc (60 mL  $\times$  3). The combined organic layer was washed with saturated solution of NaCl (60 mL  $\times$  3), dried over  $\text{MgSO}_4$  and concentrated to give compound **3** (0.602 g, yield: 68.9%.)  $^1\text{H}$  NMR (400 MHz, deuteriated dimethyl sulfoxide ( $\text{DMSO}-d_6$ ))  $\delta$  14.51 (s, 1H), 8.84 (s, 1H), 8.45 (s, 1H). ESI-MS  $m/z$ : 153.00 [ $\text{M} - \text{H}$ ] $^-$ .

#### 4.1.2. General procedure A for the synthesis of compounds (**4**)

A suspension of compound **3** (6.5 mmol) and  $\text{Cs}_2\text{CO}_3$  (13.0 mol) in dry DMF (25 mL) was stirred at  $0\text{ }^\circ\text{C}$  for 30 min, and then iodide alkane (7.8 mmol) was added. After stirring overnight, the reaction mixture was extracted with EtOAc (60 mL  $\times$  3), washed with water, dried over  $\text{Na}_2\text{SO}_4$ , and concentrated *in vacuo* to give compound **4**.

##### 4.1.2.1. 4-chloro-1-methyl-1H-pyrazolo[3,4-d]pyrimidine (**4a**)

Compound **3** (1.0 g, 6.5 mmol) was reacted with iodomethane (1.1 g, 7.8 mmol) to give compound **4a** (0.42 g, yield: 38.5%). <sup>1</sup>H NMR (400 MHz, DMSO-*d*<sub>6</sub>) δ 8.83(s, 1H), 8.41(s, 1H), 4.06(s, 3H). ESI-MS, *m/z*: 169.3[M+H]<sup>+</sup>.

#### 4.1.2.2. 4-chloro-1-ethyl-1H-pyrazolo[3,4-d]pyrimidine (**4b**)

Compound **3** (1.0 g, 6.5 mmol) was reacted with iodoethane (1.3 g, 8.1 mmol) to give compound **4b** (0.40 g, yield: 33.6%). <sup>1</sup>H NMR (400 MHz, CDCl<sub>3</sub>) δ 8.77(s, 1H), 8.17(s, 1H), 4.57(q, *J* = 7.2 Hz, 2H), 1.56(t, *J* = 7.2 Hz, 3H). ESI-MS, *m/z*: 183.4 [M+H]<sup>+</sup>.

#### 4.1.2.3. 4-chloro-1-isopropyl-1H-pyrazolo[3,4-d]pyrimidine (**4c**)

Compound **3** (1.0 g, 6.5 mmol) was reacted with 2-iodopropane (1.5 g, 8.8 mmol) to give compound **4b** (0.28 g, yield: 21.7%). <sup>1</sup>H NMR (400 MHz, CDCl<sub>3</sub>) δ 8.77(s, 1H), 8.17(s, 1H), 4.57(q, *J* = 7.2 Hz, 2H), 1.56(t, *J* = 7.2 Hz, 3H). ESI-MS, *m/z*: 183.4 [M+H]<sup>+</sup>. <sup>1</sup>H NMR (400 MHz, CDCl<sub>3</sub>) δ 8.69(s, 1H), 8.10(s, 1H), 5.19-5.29(m, 1H), 1.56(d, *J* = 6.8 Hz, 6H). ESI-MS, *m/z*: 197.3 [M+H]<sup>+</sup>.

#### 4.1.3. General procedure B for the synthesis of compounds (**5**)

To the mixture of 4-amino-3-nitrophenol (1.0 g, 6.4 mmol) in DMF (50 mL), Cs<sub>2</sub>CO<sub>3</sub> (3.12 g, 9.6 mmol) was added under the protection of nitrogen. The reaction mixture was stirred at r.t. for 1.5–2 h, and then compound **4** (6.4 mmol) was added slowly. After stirring overnight, the reaction mixture was diluted with EtOAc (50 mL), washed with water and brine, dried over Na<sub>2</sub>SO<sub>4</sub> and concentrated to give compound **5** as an orange solid.

##### 4.1.3.1. 4-((1-methyl-1H-pyrazolo[3,4-d]pyrimidin-4-yl)oxy)-2-nitroaniline (**5a**)

Compound **4a** (1.08 g, 6.4 mmol) was reacted with 4-amino-3-nitrophenol (0.99 g, 6.4 mmol) to give compound **5a** as an orange solid (1.51 g, yield: 82.3%). <sup>1</sup>H NMR (400 MHz, CDCl<sub>3</sub>) δ 8.55 (s, 1H), 8.09 (s, 1H), 8.07 (d, *J* = 2.4 Hz, 1H), 7.32-7.35 (m, 1H), 6.94 (d, *J* = 8.8 Hz, 1H), 6.20 (s, 2H), 4.16 (s, 3H). ESI-MS, *m/z*: 287.5 [M+H]<sup>+</sup>.

##### 4.1.3.2. 4-((1-ethyl-1H-pyrazolo[3,4-d]pyrimidin-4-yl)oxy)-2-nitroaniline (**5b**)

Compound **4b** (1.05 g, 5.7 mmol) was reacted with 4-amino-3-nitrophenol (0.88 g, 5.7 mmol) to give compound **5b** as an orange solid (1.36 g, yield: 79.7%). <sup>1</sup>H NMR (400 MHz, CDCl<sub>3</sub>) δ 8.54(s, 1H), 8.09(s, 1H), 8.07(d, *J* = 2.8 Hz, 1H), 7.34(dd, *J* = 2.8, 9.2 Hz, 1H), 6.93(d, *J* = 9.2 Hz, 1H), 6.17(s,

2H), 4.57(q,  $J = 7.2$  Hz, 2H), 1.57(t,  $J = 7.2$  Hz, 3H). ESI-MS,  $m/z$ : 301.4 [M+H]<sup>+</sup>.

#### 4.1.3.3. 4-((1-isopropyl-1H-pyrazolo[3,4-d]pyrimidin-4-yl)oxy)-2-nitroaniline (**5c**)

Compound **4c** (1.25 g, 6.4 mmol) was reacted with 4-amino-3-nitrophenol (0.99 g, 6.4 mmol) to give compound **5c** as an orange solid (1.49 g, yield: 74.3%). <sup>1</sup>H NMR (400 MHz, CDCl<sub>3</sub>) δ 8.53(s, 1H), 8.09(s, 1H), 8.07(d,  $J = 2.4$  Hz, 1H), 7.34(dd,  $J = 2.4, 9.2$  Hz, 1H), 6.93(d,  $J = 9.2$  Hz, 1H), 6.16(s, 2H), 5.19-5.29(m, 1H), 1.63(d,  $J = 6.8$  Hz, 6H). ESI-MS,  $m/z$ : 315.7[M+H]<sup>+</sup>.

#### 4.1.4. General procedure C for the synthesis of compounds (**6**)

To a cooled (0 °C) flask charged with CH<sub>2</sub>Cl<sub>2</sub> (18 mL) and compound **5** (3.49 mmol), trifluoroacetic anhydride (0.93 mL, 6.59 mmol) was added dropwise over 15 min and the mixture was stirred for 45 min. After that, hexadecyl trimethyl ammonium bromide (0.63 g, 1.73 mmol), dimethyl sulfate (0.66 mL, 6.94 mmol), and 50% NaOH aqueous (14 mL) were added. The mixture was allowed to warm to rt and stirred for 16 h. Then the mixture was diluted with CH<sub>2</sub>Cl<sub>2</sub>, washed with water, dried over Na<sub>2</sub>SO<sub>4</sub>, filtered, and concentrated *in vacuo*. The crude residue was purified by recrystallization from ethanol-water to give **5** as fine red needles.

##### 4.1.4.1. N-methyl-4-((1-methyl-1H-pyrazolo[3,4-d]pyrimidin-4-yl)oxy)-2-nitroaniline (**6a**)

Compound **5a** (1.0 g, 3.49 mmol) was reacted with dimethyl sulfate (0.66 mL, 6.94 mmol) to give **6a** as fine red needles (0.88 g, yield: 84.3%). <sup>1</sup>H NMR (400 MHz, CDCl<sub>3</sub>) δ 8.56 (s, 1H), 8.13 (d,  $J = 2.8$  Hz, 2H), 8.09 (s, 1H), 7.46 (dd,  $J = 9.2, 2.8$  Hz, 1H), 6.98 (d,  $J = 9.2$  Hz, 1H), 4.16 (s, 3H), 3.10 (s, 3H). ESI-MS  $m/z$ : 301.5 [M+H]<sup>+</sup>.

##### 4.1.4.2. 4-((1-ethyl-1H-pyrazolo[3,4-d]pyrimidin-4-yl)oxy)-N-methyl-2-nitroaniline (**6b**)

Compound **5b** (1.0 g, 3.33 mmol) was reacted with dimethyl sulfate (0.32 mL, 3.33 mmol) to give **6b** as fine red needles (0.84 g, yield: 80.6%). <sup>1</sup>H NMR (400 MHz, CDCl<sub>3</sub>) δ 8.54(s, 1H), 8.13(d,  $J = 2.8$  Hz, 2H), 8.08(s, 1H), 7.45(dd,  $J = 2.8, 9.2$  Hz, 1H), 6.98(d,  $J = 9.2$  Hz, 1H), 4.57(q,  $J = 7.2$  Hz, 2H), 3.11(d,  $J = 5.2$  Hz, 3H), 1.57(t,  $J = 7.2$  Hz, 3H). ESI-MS,  $m/z$ : 315.3 [M+H]<sup>+</sup>.

##### 4.1.4.3. 4-((1-isopropyl-1H-pyrazolo[3,4-d]pyrimidin-4-yl)oxy)-N-methyl-2-nitroaniline (**6c**)

Compound **5c** (1.0 g, 3.18 mmol) was reacted with dimethyl sulfate (0.31 mL, 3.18 mmol) to give **6c** as fine red needles (0.81 g, yield: 77.8%). <sup>1</sup>H NMR (400 MHz, CDCl<sub>3</sub>) δ 8.53(s, 1H), 8.13(d,  $J =$

2.4 Hz, 3H), 8.07(s, 1H), 7.45(dd,  $J = 2.8, 9.2$  Hz, 1H), 6.98(d,  $J = 9.2$  Hz, 1H), 5.19-5.29(m, 1H), 3.10(d,  $J = 5.2$  Hz, 3H), 1.63(d,  $J = 6.8$  Hz, 6H). ESI-MS,  $m/z$ : 329.7[M+H]<sup>+</sup>.

#### 4.1.5. General procedure D for the synthesis of compounds (7)

To a flask charged with compound **5** or **6** (17.4 mmol) in EtOH (300 mL), 10% Pt/C (1.56 g) was added, then a solution of hydrazine hydrate (4.22 mL, 87 mmol) in EtOH (70 mL) was added dropwise over 30 min, and the mixture was stirred for 3 h at rt. The mixture was filtered, diluted with EtOAc (100 mL), washed with water and brine, dried over Na<sub>2</sub>SO<sub>4</sub> and concentrated to give compound **7** as a brown solid.

##### 4.1.5.1 4-((1-methyl-1H-pyrazolo[3,4-d]pyrimidin-4-yl)oxy)benzene-1,2-diamine (7a)

Compound **5a** (5.0 g, 17.4 mmol) was reacted with hydrazine hydrate (4.22 mL, 87 mmol) to give compound **7a** as a brown solid (3.42 g, yield: 76.7 %). <sup>1</sup>H NMR (400 MHz, DMSO-*d*<sub>6</sub>) δ 8.54 (s, 1H), 7.42 (s, 1H), 6.57 (d,  $J = 8.4$  Hz, 1H), 6.42 (d,  $J = 2.4$  Hz, 1H), 6.30 (dd,  $J = 2.4, 8.4$  Hz, 1H), 4.75 (s, 2H), 4.56 (s, 2H), 4.00 (s, 3H). ESI-MS,  $m/z$ : 257.3 [M+H]<sup>+</sup>.

##### 4.1.5.2 *N*<sup>1</sup>-methyl-4-((1-methyl-1H-pyrazolo[3,4-d]pyrimidin-4-yl)oxy)benzene-1,2-diamine (7b)

Compound **6a** (5.0 g, 16.7 mmol) was reacted with hydrazine hydrate (4.02 mL, 83 mmol) to give compound **7b** as a brown solid (3.38 g, yield: 74.8%). <sup>1</sup>H NMR (400 MHz, DMSO-*d*<sub>6</sub>) δ 8.53 (s, 1H), 7.45 (s, 1H), 6.40-6.48 (m, 3H), 4.82 (s, 3H), 3.99 (s, 3H), 2.76 (s, 3H). ESI-MS,  $m/z$ : 271.6 [M+H]<sup>+</sup>.

##### 4.1.5.3 4-((1-ethyl-1H-pyrazolo[3,4-d]pyrimidin-4-yl)oxy)-*N*<sup>1</sup>-methylbenzene-1,2-diamine (7c)

Compound **6b** (5.0 g, 15.9 mmol) was reacted with hydrazine hydrate (3.83 mL, 79 mmol) to give compound **7c** as a brown solid (3.22 g, yield: 71.4%). <sup>1</sup>H NMR (400 MHz, CDCl<sub>3</sub>) δ 8.53(s, 1H), 7.44(s, 1H), 6.41-6.47(m, 3H), 4.79(s, 3H), 4.42(q,  $J = 7.2$  Hz, 2H), 2.76(s, 3H), 1.57(t,  $J = 7.2$  Hz, 3H). ESI-MS,  $m/z$ : 285.4 [M+H]<sup>+</sup>.

##### 4.1.5.4 4-((1-isopropyl-1H-pyrazolo[3,4-d]pyrimidin-4-yl)oxy)-*N*<sup>1</sup>-methylbenzene-1,2-diamine (7d)

Compound **6c** (5.0 g, 15.2 mmol) was reacted with hydrazine hydrate (3.64 mL, 75 mmol) to give compound **7d** as a brown solid (3.14 g, yield: 71.4%). <sup>1</sup>H NMR (400 MHz, DMSO-*d*<sub>6</sub>) δ 8.53(s, 1H), 7.42(s, 1H), 6.46-6.47(m, 1H), 6.43-6.44(m, 2H), 5.07-5.14(m, 1H), 4.78(s, 3H), 2.76(s, 3H), 1.47(d,  $J$

= 6.4 Hz, 6H). ESI-MS,  $m/z$ : 299.7[M+H]<sup>+</sup>.

#### 4.1.6. General procedure E for the synthesis of compounds (8, 9, 10, 11)

To a solution of compound **7** (0.78 mmol) in CH<sub>3</sub>CN (15 mL), a solution of isothiocyanate (0.78 mmol) in CH<sub>3</sub>CN (1 mL) was added dropwise over 5 min. The reaction mixture was stirred 18 h at rt. After that, the reaction was diluted with additional CH<sub>3</sub>CN (10 mL), followed by addition of DIC (0.147 g, 1.17 mmol). Then, the reaction was heated at 120 °C for 6 h, cooled to rt, and concentrated *in vacuo*. The crude mixture was then partitioned between EtOAc and water. The combined organic layer was washed with brine, dried over Na<sub>2</sub>SO<sub>4</sub>, and concentrated *in vacuo*. The residue was purified by silica gel column chromatography using petroleum ether-EtOAc to yield the title compound as a white solid.

##### 4.1.6.1. 5-((1-methyl-1H-pyrazolo[3,4-d]pyrimidin-4-yl)oxy)-N-phenyl-1H-benzo[d]imidazol-2-amine (8a)

Compound **7a** (0.2 g, 0.78 mmol) was reacted with phenyl isothiocyanate (0.105 g, 0.78 mmol) to give **8a** as a white solid (0.086 g, yield: 31.2%). mp: 128-131 °C. <sup>1</sup>H NMR (400 MHz, DMSO-*d*<sub>6</sub>) δ 11.06 (s, 1H), 9.53 (s, 1H), 8.55 (s, 1H), 7.70-7.77 (m, 3H), 7.24-7.40 (m, 4H), 6.93-6.96 (m, 2H), 4.03 (s, 3H). <sup>13</sup>C NMR (101 MHz, DMSO-*d*<sub>6</sub>) δ 164.5, 155.5, 155.3, 140.9, 131.4, 129.2, 121.3, 117.6, 102.1, 34.4. FT-IR (ν<sub>max</sub>, cm<sup>-1</sup>): 3649 (NH), 3629 (NH), 3064 (CH, aromatic). ESI-MS  $m/z$ : 358.6 [M+H]<sup>+</sup>. HRMS (ESI,  $m/z$ ) calcd. for C<sub>19</sub>H<sub>15</sub>N<sub>7</sub>O [M+H]<sup>+</sup> 358.1411; found, 358.1412.

##### 4.1.6.2. 5-((1-methyl-1H-pyrazolo[3,4-d]pyrimidin-4-yl)oxy)-N-(*o*-tolyl)-1H-benzo[d]imidazol-2-amine (8b)

Compound **7a** (0.2 g, 0.78 mmol) was reacted with 2-methylphenyl isothiocyanate (0.12 g, 0.78 mmol) to give **8b** as a white solid (0.10 mg, yield: 35.3%). mp: 124-136 °C. <sup>1</sup>H NMR (400 MHz, DMSO-*d*<sub>6</sub>) δ 11.00 (s, 1H), 8.47-8.54 (m, 2H), 8.11-8.23 (m, 1H), 7.69-7.72 (m, 1H), 7.36 (d, *J* = 7.6 Hz, 1H), 7.21-7.22 (m, 3H), 6.90-6.98 (m, 2H), 4.03 (s, 3H), 2.31 (s, 3H). <sup>13</sup>C NMR (101 MHz, DMSO-*d*<sub>6</sub>) δ 164.5, 155.5, 155.2, 138.6, 131.4, 130.8, 126.9, 123.0, 120.6, 102.1, 34.4, 18.2. FT-IR (ν<sub>max</sub>, cm<sup>-1</sup>): 3650 (NH), 3563 (NH), 3050 (CH, aromatic). ESI-MS  $m/z$ : 372.5 [M+H]<sup>+</sup>. HRMS (ESI,  $m/z$ ) calcd. for C<sub>20</sub>H<sub>17</sub>N<sub>7</sub>O [M+H]<sup>+</sup> 372.1368; found, 372.1570.

##### 4.1.6.3.

5-((1-methyl-1H-pyrazolo[3,4-d]pyrimidin-4-yl)oxy)-N-(m-tolyl)-1H-benzo[d]imidazol-2-amine (**8c**)

Compound **7a** (0.2 g, 0.78 mmol) was reacted with 3-methylphenyl isothiocyanate (0.12 g, 0.78 mmol) to give **8c** as a white solid (0.099 g, yield: 34.9%). mp: 118-120 °C. <sup>1</sup>H NMR (400 MHz, DMSO-*d*<sub>6</sub>) δ 11.04 (s, 1H), 9.44 (s, 1H), 8.55 (s, 1H), 7.71-7.76 (m, 1H), 7.55-7.58 (m, 2H), 7.18-7.42 (m, 3H), 6.92 (s, 1H), 6.77 (d, *J* = 7.2 Hz, 1H), 4.03 (s, 3H), 2.32 (s, 3H). <sup>13</sup>C NMR (101 MHz, DMSO-*d*<sub>6</sub>) δ 164.4, 155.5, 155.3, 152.1, 146.6, 140.8, 138.4, 131.4, 129.1, 122.2, 118.3, 115.1, 114.1, 102.1, 34.4, 21.7. FT-IR (ν<sub>max</sub>, cm<sup>-1</sup>): 3627 (NH), 3587 (NH), 3004 (CH, aromatic). ESI-MS *m/z*: 372.5 [M+H]<sup>+</sup>. HRMS (ESI, *m/z*) calcd. C<sub>20</sub>H<sub>17</sub>N<sub>7</sub>O [M+H]<sup>+</sup> 372.1368; found, 372.1572.

4.1.6.4. N-(3-chlorophenyl)-5-((1-methyl-1H-pyrazolo[3,4-d]pyrimidin-4-yl)oxy)-1H-benzo[d]imidazol-2-amine (**8d**)

Compound **7a** (0.2 g, 0.78 mmol) was reacted with 3-chlorophenyl isothiocyanate (0.13 g, 0.78 mmol) to give **8d** as a white solid (0.11 g, yield: 37.2%). mp: 127-130 °C. <sup>1</sup>H NMR (400 MHz, DMSO-*d*<sub>6</sub>) δ 11.2 (s, 1H), 9.76-9.80 (m, 1H), 8.55 (s, 1H), 8.07 (s, 1H), 7.75-7.81 (m, 1H), 7.58 (d, *J* = 8.4 Hz, 1H), 7.26-7.48 (m, 3H), 6.97-6.99 (m, 3H), 4.03 (s, 3H). <sup>13</sup>C NMR (101 MHz, DMSO-*d*<sub>6</sub>) δ 164.3, 155.4, 155.2, 151.2, 146.9, 141.9, 133.8, 131.3, 130.9, 121.4, 117.4, 116.6, 114.8, 102.1, 34.4. FT-IR (ν<sub>max</sub>, cm<sup>-1</sup>): 3675 (NH), 3640 (NH), 3092 (CH, aromatic). ESI-MS *m/z*: 392.5 [M+H]<sup>+</sup>. HRMS (ESI, *m/z*) calcd. for C<sub>19</sub>H<sub>14</sub>N<sub>7</sub>O Cl [M+H]<sup>+</sup> 392.1022; found, 392.1020.

4.1.6.5. N-(4-chlorophenyl)-5-((1-methyl-1H-pyrazolo[3,4-d]pyrimidin-4-yl)oxy)-1H-benzo[d]imidazol-2-amine (**8e**)

Compound **7a** (0.2 g, 0.78 mmol) was reacted with 3-chlorophenyl isothiocyanate (0.13 g, 0.78 mmol) to give **8e** as a white solid (0.11 g, yield: 36.4%). mp: 180-183 °C. <sup>1</sup>H NMR (400 MHz, DMSO-*d*<sub>6</sub>) δ 11.16 (s, 1H), 9.71 (s, 1H), 8.54 (s, 1H), 7.73-7.83 (m, 3H), 7.25-7.42 (m, 4H), 6.94 (s, 1H), 4.03 (s, 3H). <sup>13</sup>C NMR (101 MHz, DMSO-*d*<sub>6</sub>) δ 164.4, 155.5, 155.3, 140.0, 131.4, 129.0, 124.6, 119.1, 102.1, 34.4. FT-IR (ν<sub>max</sub>, cm<sup>-1</sup>): 3652 (NH), 3558 (NH), 3052 (CH, aromatic). ESI-MS *m/z*: 392.5 [M+H]<sup>+</sup>. HRMS (ESI, *m/z*) calcd. for C<sub>19</sub>H<sub>14</sub>N<sub>7</sub>O Cl [M+H]<sup>+</sup> 392.1022; found, 392.1025.

4.1.6.6. 1-methyl-5-((1-methyl-1H-pyrazolo[3,4-d]pyrimidin-4-yl)oxy)-N-phenyl-1H-benzo[d]imidazol-2-amine (**9a**)

Compound **7b** (0.2 g, 0.74 mmol) was reacted with phenyl isothiocyanate (0.10 g, 0.74 mmol) to

give **9a** as a white solid (0.081 g, yield: 29.8%). mp: 274-275 °C. <sup>1</sup>H NMR (400 MHz, DMSO-*d*<sub>6</sub>) δ 9.02 (s, 1H), 8.54 (s, 1H), 7.87 (d, *J* = 8.4 Hz, 2H), 7.74 (s, 1H), 7.39 (d, *J* = 8.8 Hz, 1H), 7.33 (t, *J* = 8.0 Hz, 3H), 6.94-7.00 (m, 2H), 4.03 (s, 3H), 3.77 (s, 3H). <sup>13</sup>C NMR (101 MHz, DMSO-*d*<sub>6</sub>) δ 164.4, 155.5, 155.3, 152.1, 147.2, 142.7, 141.1, 132.9, 131.4, 129.0, 121.6, 118.5, 113.6, 109.8, 108.7, 102.1, 34.4, 29.6; FT-IR (ν<sub>max</sub>, cm<sup>-1</sup>): 3304 (NH), 3100 (CH, aromatic). ESI-MS, *m/z*: 372.4 [M+H]<sup>+</sup>. HRMS (ESI, *m/z*) calcd. for C<sub>20</sub>H<sub>17</sub>N<sub>7</sub>O [M+H]<sup>+</sup> 372.1568; found, 372.1571.

#### 4.1.6.7.

*1-methyl-5-((1-methyl-1H-pyrazolo[3,4-d]pyrimidin-4-yl)oxy)-N-(o-tolyl)-1H-benzo[d]imidazol-2-amine (9b)*

Compound **7b** (0.2 g, 0.74 mmol) was reacted with 2-methylphenyl isothiocyanate (0.11 g, 0.74 mmol) to give **9b** as a white solid (0.10 g, yield: 35.2%). mp: 193-195 °C. <sup>1</sup>H NMR (400 MHz, DMSO-*d*<sub>6</sub>) δ 8.52 (s, 1H), 8.27 (s, 1H), 7.73 (s, 1H), 7.58 (d, *J* = 8.0 Hz, 1H), 7.36 (d, *J* = 8.4 Hz, 1H), 7.18-7.25 (m, 3H), 7.06 (t, *J* = 7.6 Hz, 1H), 6.95 (d, *J* = 8.4 Hz, 1H), 4.02 (s, 3H), 3.74 (s, 3H), 2.27 (s, 3H). <sup>13</sup>C NMR (101 MHz, DMSO-*d*<sub>6</sub>) δ 164.5, 155.5, 155.3, 153.9, 147.2, 143.0, 139.1, 133.5, 131.7, 131.46, 130.8, 126.7, 124.5, 124.2, 113.3, 109.6, 108.6, 102.2, 34.4, 29.6, 18.4. FT-IR (ν<sub>max</sub>, cm<sup>-1</sup>): 3340 (NH), 3094 (CH, aromatic). ESI-MS *m/z*: 386.5 [M+H]<sup>+</sup>. HRMS (ESI, *m/z*) calcd. for C<sub>21</sub>H<sub>19</sub>N<sub>7</sub>O [M+H]<sup>+</sup> 386.1724; found, 386.1727.

*4.1.6.8.1-methyl-5-((1-methyl-1H-pyrazolo[3,4-d]pyrimidin-4-yl)oxy)-N-(m-tolyl)-1H-benzo[d]imidazol-2-amine (9c)*

Compound **7b** (0.2 g, 0.74 mmol) was reacted with 3-methylphenyl isothiocyanate (0.11 g, 0.74 mmol) to give **9c** as a white solid (0.09 g, yield: 33.4%). mp: 225-228 °C. <sup>1</sup>H NMR (400 MHz, DMSO-*d*<sub>6</sub>) δ 8.92 (s, 1H), 8.53 (s, 1H), 7.73 (s, 1H), 7.70 (d, *J* = 8.0 Hz, 1H), 7.65 (s, 1H), 7.38 (d, *J* = 8.4 Hz, 1H), 7.32 (s, 1H), 7.2 (t, *J* = 7.6 Hz, 1H), 6.99 (d, *J* = 8.4 Hz, 1H), 6.79 (d, *J* = 7.2 Hz, 1H), 4.03 (s, 3H), 3.75 (s, 3H), 2.50 (s, 3H). <sup>13</sup>C NMR (101 MHz, DMSO-*d*<sub>6</sub>) δ 164.5, 155.5, 155.3, 152.2, 147.2, 142.8, 141.0, 138.1, 132.9, 131.4, 128.9, 122.4, 118.9, 115.7, 113.6, 109.8, 108.7, 102.1, 34.4, 29.6, 21.7. FT-IR (ν<sub>max</sub>, cm<sup>-1</sup>): 3278 (NH), 3092 (CH, aromatic). ESI-MS, *m/z*: 386.4 [M+H]<sup>+</sup>. HRMS (ESI, *m/z*) calcd. for C<sub>21</sub>H<sub>19</sub>N<sub>7</sub>O [M+H]<sup>+</sup> 386.1724; found, 386.1726.

*4.1.6.9. N-(3-chlorophenyl)-1-methyl-5-((1-methyl-1H-pyrazolo[3,4-d]pyrimidin-4-yl)oxy)-1H-benzo*

[*d*]imidazol-2-amine (**9d**).

Compound **7b** (0.2 g, 0.74 mmol) was reacted with 3-chlorophenyl isothiocyanate (0.13 g, 0.74 mmol) to give **9d** as a white solid (0.117g, yield: 38.9%). mp: 248-250 °C. <sup>1</sup>H NMR (400 MHz, DMSO-*d*<sub>6</sub>) δ 9.25 (s, 1H), 8.54 (s, 1H), 8.13 (s, 1H), 7.76-7.77 (m, 2H), 7.33-7.43 (m, 3H), 6.99-7.03 (m, 2H), 4.03 (s, 3H), 3.78 (s, 3H). <sup>13</sup>C NMR (101 MHz, DMSO-*d*<sub>6</sub>) δ 164.4, 155.5, 155.3, 151.5, 147.3, 142.6, 142.4, 133.5, 132.8, 131.4, 130.6, 121.1, 117.6, 116.8, 114.1, 110.1, 109.0, 102.2, 34.4, 29.7. FT-IR (ν<sub>max</sub>, cm<sup>-1</sup>): 3353 (NH), 3096 (CH, aromatic). ESI-MS, *m/z*: 406.4 [M+H]<sup>+</sup>. HRMS (ESI, *m/z*) calcd. for C<sub>20</sub>H<sub>16</sub>N<sub>7</sub>OCl [M+H]<sup>+</sup> 406.1178; found, 406.1181.

4.1.6.10. *N*-(4-chlorophenyl)-1-methyl-5-((1-methyl-1*H*-pyrazolo[3,4-*d*]pyrimidin-4-yl)oxy)-1*H*-benzo[*d*]imidazol-2-amine (**9e**)

Compound **7b** (0.2 g, 0.74 mmol) was reacted with 4-chlorophenyl isothiocyanate (0.13 g, 0.74 mmol) to give **9e** as a white solid (0.115g, yield: 38.3%). mp: 246-248 °C. <sup>1</sup>H NMR (400 MHz, DMSO-*d*<sub>6</sub>) δ 9.25 (s, 1H), 8.54 (s, 1H), 8.13 (s, 1H), 7.76-7.77 (m, 2H), 7.33-7.43 (m, 3H), 7.00-7.04 (m, 2H), 4.03 (s, 3H), 3.78 (s, 3H). <sup>13</sup>C NMR (101 MHz, DMSO-*d*<sub>6</sub>) δ 164.4, 155.5, 155.3, 151.5, 147.3, 142.6, 142.4, 133.5, 132.8, 131.4, 130.6, 121.1, 117.6, 116.8, 114.1, 110.1, 109.0, 102.2, 34.4, 29.7. FT-IR (ν<sub>max</sub>, cm<sup>-1</sup>): 3289 (NH), 3095 (CH, aromatic). ESI-MS, *m/z*: 406.4 [M+H]<sup>+</sup>. HRMS (ESI, *m/z*) calcd. for C<sub>20</sub>H<sub>16</sub>N<sub>7</sub>OCl [M+H]<sup>+</sup> 406.1178; found, 406.1179.

4.1.6.11. *N*-(4-chloro-3-(trifluoromethyl)phenyl)-1-methyl-5-((1-methyl-1*H*-pyrazolo[3,4-*d*]pyrimidin-4-yl)oxy)-1*H*-benzo[*d*]imidazol-2-amine (**9f**)

Compound **7b** (0.2 g, 0.74 mmol) was reacted with 4-chloro-3-(trifluoromethyl)phenyl isothiocyanate (0.176 g, 0.74 mmol) to give **9f** as a white solid (0.132 g, yield: 37.6%). mp: 272-275 °C. <sup>1</sup>H NMR (400 MHz, DMSO-*d*<sub>6</sub>) δ 8.53 (s, 1H), 8.42 (s, 1H), 8.31 (d, *J* = 9.2 Hz, 1H), 7.79 (s, 1H), 7.68 (d, *J* = 8.8 Hz, 1H), 7.45 (d, *J* = 8.4 Hz, 1H), 7.38 (s, 1H), 7.05 (d, *J* = 8.4 Hz, 1H), 4.03 (s, 3H), 3.79 (s, 3H). <sup>13</sup>C NMR (101 MHz, DMSO-*d*<sub>6</sub>) δ 164.4, 155.5, 155.3, 151.1, 147.4, 142.2, 140.6, 132.7, 132.3, 131.4, 126.8, 122.7, 121.7, 116.9, 114.4, 110.3, 109.2, 102.2, 34.4, 29.7. FT-IR (ν<sub>max</sub>, cm<sup>-1</sup>): 3290 (NH), 3098 (CH, aromatic). ESI-MS, *m/z*: 474.4 [M+H]<sup>+</sup>. HRMS (ESI, *m/z*) calcd for C<sub>21</sub>H<sub>15</sub>N<sub>7</sub>OClF<sub>3</sub> [M+H]<sup>+</sup> 474.1051; found, 474.1045.

4.1.6.12.

*1-methyl-5-((1-methyl-1H-pyrazolo[3,4-d]pyrimidin-4-yl)oxy)-N-(p-tolyl)-1H-benzo[d]imidazol-2-amine (9g)*

Compound **7b** (0.2 g, 0.74 mmol) was reacted with 4-methylphenyl isothiocyanate (0.110 g, 0.74 mmol) to give **9g** as a white solid (0.110 g, yield: 38.8%). mp: 220-223 °C. <sup>1</sup>H NMR (400 MHz, DMSO-*d*<sub>6</sub>) δ 8.98 (s, 1H), 8.53 (s, 1H), 7.73-7.74 (m, 3H), 7.36-7.38 (d, *J* = 8.0 Hz, 1H), 7.29 (s, 1H), 7.12-7.14 (m, 2H), 6.97-6.99 (m, 1H), 4.02 (s, 3H), 3.75 (s, 3H), 2.26 (s, 3H). <sup>13</sup>C NMR (101 MHz, DMSO-*d*<sub>6</sub>) δ 164.5, 155.5, 155.3, 152.3, 147.2, 138.4, 132.9, 131.4, 130.6, 129.4, 118.8, 113.6, 109.6, 108.6, 102.1, 34.4, 29.6, 20.8. FT-IR (ν<sub>max</sub>, cm<sup>-1</sup>): 3290 (NH), 3091 (CH, aromatic). ESI-MS, *m/z*: 386.5 [M+H]<sup>+</sup>. HRMS (ESI, *m/z*) calcd. for C<sub>21</sub>H<sub>19</sub>N<sub>7</sub>O [M+H]<sup>+</sup> 386.1724; found, 386.1726.

*4.1.6.13. 4-((1-methyl-5-((1-methyl-1H-pyrazolo[3,4-d]pyrimidin-4-yl)oxy)-1H-benzo[d]imidazol-2-yl)amino)benzotrile (9h)*

Compound **7b** (0.2 g, 0.74 mmol) was reacted with 4-cyanophenyl isothiocyanate (0.118 g, 0.74 mmol) to give **9h** as a white solid (0.092 g, yield: 31.5%). mp: 239-241 °C. <sup>1</sup>H NMR (400 MHz, DMSO-*d*<sub>6</sub>) δ 9.61 (s, 1H), 8.54 (s, 1H), 8.07 (d, *J* = 8.8 Hz, 2H), 7.82 (s, 1H), 7.78 (d, *J* = 8.8 Hz, 2H), 7.47 (d, *J* = 8.4 Hz, 1H), 7.41 (d, *J* = 2.0 Hz, 1H), 7.07 (dd, *J* = 8.4, 2.0 Hz, 1H), 4.04 (s, 3H), 3.81 (s, 3H). <sup>13</sup>C NMR (101 MHz, DMSO-*d*<sub>6</sub>) δ 164.3, 155.5, 155.3, 150.7, 147.4, 145.4, 142.2, 133.6, 132.7, 131.4, 120.0, 118.1, 114.6, 110.4, 109.4, 102.7, 102.2, 34.3, 29.9; FT-IR (ν<sub>max</sub>, cm<sup>-1</sup>): 3282 (NH), 3090 (CH, aromatic). ESI-MS, *m/z*: 395.4 [M+H]<sup>+</sup>. HRMS (ESI, *m/z*) calcd. for C<sub>21</sub>H<sub>16</sub>ON<sub>8</sub> [M+H]<sup>+</sup> 397.1520; found, 397.1520.

*4.1.6.14. 1-methyl-5-((1-methyl-1H-pyrazolo[3,4-d]pyrimidin-4-yl)oxy)-N-(3,4,5-trimethoxyphenyl)-1H-benzo[d]imidazol-2-amine (9i)*

Compound **7b** (0.2 g, 0.74 mmol) was reacted with 3,4,5-trimethoxyphenyl isothiocyanate (0.167 g, 0.74 mmol) to give **9i** as a brown solid (0.103 g, yield: 30.1%). mp: 232-234 °C. <sup>1</sup>H NMR (400 MHz, DMSO-*d*<sub>6</sub>) δ 8.94 (s, 1H), 8.53 (s, 1H), 7.76 (s, 1H), 7.38 (d, *J* = 8.4 Hz, 1H), 7.31 (s, 3H), 7.29 (d, *J* = 2.4 Hz, 1H), 6.99 (dd, *J* = 8.4, 2.0 Hz, 1H), 4.03 (s, 3H), 3.79 (s, 6H), 3.75 (s, 3H), 3.64 (s, 3H). <sup>13</sup>C NMR (101 MHz, DMSO-*d*<sub>6</sub>) δ 164.5, 155.5, 155.3, 153.2, 152.2, 147.2, 142.8, 137.2, 132.8, 132.6, 131.4, 113.6, 109.9, 108.6, 102.2, 96.7, 60.6, 56.2, 34.4, 29.6. FT-IR (ν<sub>max</sub>, cm<sup>-1</sup>): 3304 (NH), 3017 (CH, aromatic). ESI-MS, *m/z*: 462.4 [M+H]<sup>+</sup>. HRMS (ESI, *m/z*) calcd. for C<sub>23</sub>H<sub>23</sub>O<sub>4</sub>N<sub>7</sub> [M+H]<sup>+</sup>

462.1885; found, 462.1886.

4.1.6.15. *N*-(4-(*tert*-butyl)phenyl)-1-methyl-5-((1-methyl-1*H*-pyrazolo[3,4-*d*]pyrimidin-4-yl)oxy)-1*H*-benzo[*d*]imidazol-2-amine (**9j**)

Compound **7b** (0.2 g, 0.74 mmol) was reacted with 4-*tert*-butylphenyl isothiocyanate (0.141 g, 0.74 mmol) to give **9j** as a white solid (0.099 g, yield: 31.3%). mp: 309-310 °C. <sup>1</sup>H NMR (400 MHz, DMSO-*d*<sub>6</sub>) δ 8.93 (s, 1H), 8.54 (s, 1H), 7.74-7.76 (m, 3H), 7.33-7.38 (m, 3H), 7.28 (d, *J* = 2.0 Hz, 1H), 6.97 (dd, *J* = 8.4, 2.4 Hz, 1H), 4.03 (s, 3H), 3.75 (s, 3H), 1.28 (s, 9H). <sup>13</sup>C NMR (101 MHz, DMSO-*d*<sub>6</sub>) δ 164.5, 155.5, 155.3, 152.5, 147.2, 144.0, 142.9, 138.5, 133.0, 131.4, 125.6, 118.5, 113.4, 109.7, 108.6, 102.2, 34.4, 34.3, 31.7, 29.6. FT-IR (ν<sub>max</sub>, cm<sup>-1</sup>): 3280 (NH), 3092 (CH, aromatic), 2961 (CH, aliphatic). ESI-MS, *m/z*: 428.7 [M+H]<sup>+</sup>. HRMS (ESI, *m/z*) calcd. for C<sub>24</sub>H<sub>25</sub>ON<sub>7</sub> [M+H]<sup>+</sup> 428.2194; found, 428.2195.

4.1.6.16. *N*-(2-chlorophenyl)-1-methyl-5-((1-methyl-1*H*-pyrazolo[3,4-*d*]pyrimidin-4-yl)oxy)-1*H*-benzo[*d*]imidazol-2-amine (**9k**)

Compound **7b** (0.2 g, 0.74 mmol) was reacted with 2-chlorophenyl isothiocyanate (0.125 g, 0.74 mmol) to give **9k** as a white solid (0.098 g, yield: 32.6%). mp: 242-243 °C. <sup>1</sup>H NMR (400 MHz, DMSO-*d*<sub>6</sub>) δ 8.53 (s, 1H), 8.45 (s, 1H), 8.00 (d, *J* = 8.0 Hz, 1H), 7.80 (s, 1H), 7.51 (d, *J* = 7.6 Hz, 1H), 7.44 (d, *J* = 8.4 Hz, 1H), 7.36 (t, *J* = 7.6 Hz, 1H), 7.30 (d, *J* = 1.6 Hz, 1H), 7.12 (t, *J* = 8.4 Hz, 1H), 7.02 (dd, *J* = 8.8, 2.4 Hz, 1H), 4.03 (s, 3H), 3.78 (s, 3H). <sup>13</sup>C NMR (101 MHz, DMSO-*d*<sub>6</sub>) δ 164.4, 155.5, 155.3, 152.5, 147.3, 142.4, 137.7, 133.2, 131.4, 129.9, 128.1, 125.4, 124.7, 123.8, 114.1, 110.2, 109.2, 102.2, 34.4, 29.7. FT-IR (ν<sub>max</sub>, cm<sup>-1</sup>): 3419 (NH), 3098 (CH, aromatic). ESI-MS *m/z*: 406.6 [M+H]<sup>+</sup>. HRMS (ESI, *m/z*) calcd. for C<sub>20</sub>H<sub>16</sub>N<sub>7</sub>OCl [M+H]<sup>+</sup> 406.1178; found, 406.1180.

4.1.6.17.

*N*-(3-bromophenyl)-1-methyl-5-((1-methyl-1*H*-pyrazolo[3,4-*d*]pyrimidin-4-yl)oxy)-1*H*-benzo[*d*]imidazol-2-amine (**9l**)

Compound **7b** (0.2 g, 0.74 mmol) was reacted with 3-bromophenyl isothiocyanate (0.158 g, 0.74 mmol) to give **9l** as a white solid (0.122 g, yield: 36.5%). mp: 245-246 °C. <sup>1</sup>H NMR (400 MHz, DMSO-*d*<sub>6</sub>) δ 9.30 (s, 1H), 8.54 (s, 1H), 8.26 (s, 1H), 7.85 (d, *J* = 9.2 Hz, 1H), 7.77 (s, 1H), 7.38-7.43 (m, 2H), 7.29 (t, *J* = 8.0 Hz, 1H), 7.13 (d, *J* = 8.0 Hz, 1H), 7.02 (dd, *J* = 8.4, 2.4 Hz, 1H), 4.03 (s, 3H), 3.79 (s, 3H). <sup>13</sup>C NMR (101 MHz, DMSO-*d*<sub>6</sub>) δ 164.4, 155.5, 155.3, 151.5, 147.3, 142.8, 142.5, 132.8,

131.4, 130.9, 124.0, 122.0, 120.4, 117.2, 114.1, 110.1, 109.0, 102.2, 34.4, 29.7. FT-IR ( $\nu_{\max}$ ,  $\text{cm}^{-1}$ ): 3338 (NH), 3095 (CH, aromatic). ESI-MS,  $m/z$ : 448.3  $[\text{M}+\text{H}]^+$ . HRMS (ESI,  $m/z$ ) calcd. for  $\text{C}_{20}\text{H}_{16}\text{N}_7\text{OBr}$   $[\text{M}+\text{H}]^+$  450.0673; found, 450.0672.

#### 4.1.6.18.

*N*-(4-bromophenyl)-1-methyl-5-((1-methyl-1H-pyrazolo[3,4-d]pyrimidin-4-yl)oxy)-1H-benzo[d]imidazol-2-amine (**9m**).

Compound **7b** (0.2 g, 0.74 mmol) was reacted with 4-bromophenyl isothiocyanate (0.158 g, 0.74 mmol) to give **9m** as a white solid (0.112 g, yield: 36.5%). mp: 251-253 °C.  $^1\text{H}$  NMR (400 MHz,  $\text{DMSO}-d_6$ )  $\delta$  9.20 (s, 1H), 9.53 (s, 1H), 7.88 (d,  $J = 8.8$  Hz, 2H), 7.76 (s, 1H), 7.50 (d,  $J = 8.8$  Hz, 2H), 7.41 (d,  $J = 8.8$  Hz, 1H), 7.34 (d,  $J = 1.6$  Hz, 1H), 7.01 (dd,  $J = 8.4, 2.0$  Hz, 1H), 4.03 (s, 3H), 3.77 (s, 3H).  $^{13}\text{C}$  NMR (101 MHz,  $\text{DMSO}-d_6$ )  $\delta$  164.4, 155.5, 155.3, 151.7, 147.3, 142.6, 140.5, 132.8, 131.7, 131.4, 120.3, 113.9, 112.9, 109.9, 108.9, 102.2, 34.4, 29.7. FT-IR ( $\nu_{\max}$ ,  $\text{cm}^{-1}$ ): 3278 (NH), 3094 (CH, aromatic). ESI-MS,  $m/z$ : 448.3  $[\text{M}+\text{H}]^+$ . HRMS (ESI,  $m/z$ ) calcd for  $\text{C}_{20}\text{H}_{16}\text{N}_7\text{OBr}$   $[\text{M}+\text{H}]^+$  450.0672; found, 450.0670.

#### 4.1.6.19.

*N*-(4-fluorophenyl)-1-methyl-5-((1-methyl-1H-pyrazolo[3,4-d]pyrimidin-4-yl)oxy)-1H-benzo[d]imidazol-2-amine (**9n**).

Compound **7b** (0.2 g, 0.74 mmol) was reacted with 4-fluorophenyl isothiocyanate (0.113 g, 0.74 mmol) to give **9n** as a white solid (0.107 g, yield: 37.1%). mp: 274-277 °C.  $^1\text{H}$  NMR (400 MHz,  $\text{DMSO}-d_6$ )  $\delta$  9.06 (s, 1H), 8.53 (s, 1H), 7.87-7.91 (m, 2H), 7.74 (s, 1H), 7.38 (d,  $J = 8.4$  Hz, 1H), 7.31 (s, 1H), 7.17 (t,  $J = 8.6$  Hz, 2H), 6.99 (dd,  $J = 8.4, 2.4$  Hz, 1H), 4.03 (s, 3H), 3.76 (s, 3H).  $^{13}\text{C}$  NMR (101 MHz,  $\text{DMSO}-d_6$ )  $\delta$  164.5, 155.5, 155.3, 152.3, 147.3, 142.7, 137.5, 132.9, 131.4, 120.1, 115.6, 115.4, 113.7, 109.8, 108.7, 102.1, 34.4, 29.6; FT-IR ( $\nu_{\max}$ ,  $\text{cm}^{-1}$ ): 3298 (NH), 3099 (CH, aromatic). ESI-MS,  $m/z$ : 390.4  $[\text{M}+\text{H}]^+$ . HRMS (ESI,  $m/z$ ) calcd. for  $\text{C}_{20}\text{H}_{16}\text{N}_7\text{OF}$   $[\text{M}+\text{H}]^+$  390.1473; found, 390.1473.

#### 4.1.6.20.

*N*-(3,4-dichlorophenyl)-1-methyl-5-((1-methyl-1H-pyrazolo[3,4-d]pyrimidin-4-yl)oxy)-1H-benzo[d]imidazol-2-amine (**9o**)

Compound **7b** (0.2 g, 0.74 mmol) was reacted with 3,4-dichlorophenyl isothiocyanate (0.151 g, 0.74 mmol) to give **9o** as a white solid (0.125 g, yield: 38.4%). mp: 274-278 °C. <sup>1</sup>H NMR (400 MHz, DMSO-*d*<sub>6</sub>) δ 9.38 (s, 1H), 8.53 (s, 1H), 8.33 (d, *J* = 2.4 Hz, 1H), 7.85 (dd, *J* = 8.8, 2.4 Hz, 1H), 7.78 (s, 1H), 7.57 (d, *J* = 8.0 Hz, 1H), 7.40-7.44 (m, 2H), 7.04 (dd, *J* = 8.8, 2.4 Hz, 1H), 4.03 (s, 3H), 3.78 (s, 3H). <sup>13</sup>C NMR (101 MHz, DMSO-*d*<sub>6</sub>) δ 164.4, 155.5, 155.30, 151.2, 147.4, 142.3, 141.2, 132.7, 131.4, 131.3, 130.9, 122.7, 119.2, 118.4, 114.3, 110.2, 109.1, 102.1, 34.41, 29.7. FT-IR (ν<sub>max</sub>, cm<sup>-1</sup>): 3289(NH), 3097 (CH, aromatic). ESI-MS, *m/z*: 438.4 [M+H]<sup>+</sup>. HRMS (ESI, *m/z*) calcd. for C<sub>20</sub>H<sub>15</sub>N<sub>7</sub>OCl<sub>2</sub> [M+H]<sup>+</sup> 439.0710; found, 439.0712.

#### 4.1.6.21.

*N*-(2-bromo-5-fluorophenyl)-1-methyl-5-((1-methyl-1*H*-pyrazolo[3,4-*d*]pyrimidin-4-yl)oxy)-1*H*-benzo[*d*]imidazol-2-amine (**9p**)

Compound **7b** (0.2 g, 0.74 mmol) was reacted with 2--bromo-5-fluorophenyl isothiocyanate (0.172 g, 0.74 mmol) to give **9p** as a white solid (0.118 g, yield: 38.4%). mp: 83-284 °C. <sup>1</sup>H NMR (400 MHz, CDCl<sub>3</sub>) δ 8.58 (s, 1H), 8.42 (d, *J* = 10.4 Hz, 1H), 7.75 (s, 1H), 7.52-7.55 (m, 2H), 7.31 (s, 1H), 7.12 (dd, *J* = 8.4, 1.6Hz, 1H), 6.70 (td, *J* = 8.4, 2.4 Hz, 1H), 4.14 (s, 3H), 3.77 (s, 3H). <sup>13</sup>C NMR (101 MHz, CDCl<sub>3</sub>) δ 164.3, 163.8, 161.4, 155.3, 149.3, 147.8, 132.9, 132.8, 131.9, 131.3, 115.2, 111.1, 110.5, 110.2, 108.4, 107.0, 106.7, 102.5, 34.2, 29.1. FT-IR (ν<sub>max</sub>, cm<sup>-1</sup>): 3406 (NH), 3094 (CH, aromatic). ESI-MS, *m/z*: 468.3 [M-H]<sup>-</sup>. HRMS (ESI, *m/z*) calcd. for C<sub>20</sub>H<sub>15</sub>N<sub>7</sub>OBrF [M+H]<sup>+</sup> 468.0580; found, 468.0582.

#### 4.1.6.22.

*N*<sup>*l*</sup>,*N*<sup>*l*</sup>-dimethyl-*N*<sup>*l*</sup>-(1-methyl-5-((1-methyl-1*H*-pyrazolo[3,4-*d*]pyrimidin-4-yl)oxy)-1*H*-benzo[*d*]imidazol-2-yl)benzene-1,4-diamine (**9q**)

Compound **7b** (0.2 g, 0.74 mmol) was reacted with 4-dimethylaminophenyl isothiocyanate (0.132 g, 0.74 mmol) to give **9q** as a white solid (0.097 g, yield: 31.8%). mp: 242-244 °C. <sup>1</sup>H NMR (400 MHz, DMSO-*d*<sub>6</sub>) δ 8.70 (s, 1H), 8.54 (s, 1H), 7.68 (s, 1H), 7.64 (d, *J* = 9.2 Hz, 2H), 7.32 (d, *J* = 8.4 Hz, 1H), 7.23 (d, *J* = 2.4 Hz, 1H), 6.93 (dd, *J* = 8.4, 2.4 Hz, 1H), 6.76 (d, *J* = 9.2 Hz, 2H), 4.02 (s, 3H), 3.72 (s, 3H), 2.85 (s, 6H). <sup>13</sup>C NMR (101 MHz, DMSO-*d*<sub>6</sub>) δ 164.5, 155.5, 155.3, 153.2, 147.1, 146.6, 143.2, 133.2, 131.4, 131.1, 120.7, 113.5, 112.9, 109.3, 108.2, 102.1, 41.2, 34.4, 29.4. FT-IR (ν<sub>max</sub>, cm<sup>-1</sup>):

3283 (NH), 3097 (CH, aromatic). ESI-MS,  $m/z$ : 415.5  $[M+H]^+$ . HRMS (ESI,  $m/z$ ) calcd. for  $C_{22}H_{22}N_8O$   $[M+H]^+$  415.1989; found, 415.1988.

#### 4.1.6.23.

*1-methyl-5-((1-methyl-1H-pyrazolo[3,4-d]pyrimidin-4-yl)oxy)-N-(3-(trifluoromethyl)phenyl)-1H-benzo[d]imidazol-2-amine (9r)*.

Compound **7b** (0.2 g, 0.74 mmol) was reacted with 3-(trifluoromethyl)phenyl isothiocyanate (0.150 g, 0.74 mmol) to give **9r** as a white solid (0.117 g, yield: 35.9%). mp: 224-227 °C.  $^1H$  NMR (400 MHz, DMSO- $d_6$ )  $\delta$  9.40 (s, 1H), 8.54 (s, 1H), 8.31 (s, 1H), 8.22 (d,  $J$  = 8.0 Hz, 1H), 7.79 (s, 1H), 7.57 (t,  $J$  = 8.0 Hz, 1H), 7.44 (d,  $J$  = 8.4 Hz, 1H), 7.38 (d,  $J$  = 1.2 Hz, 1H), 7.30 (d,  $J$  = 7.6 Hz, 1H), 7.04 (dd,  $J$  = 8.4, 1.6 Hz, 1H), 4.03 (s, 3H), 3.80 (s, 3H).  $^{13}C$  NMR (101 MHz, DMSO- $d_6$ )  $\delta$  164.4, 155.5, 155.3, 151.5, 147.4, 142.4, 141.9, 132.8, 131.4, 130.2, 121.7, 117.7, 114.2, 110.2, 109.1, 102.2, 34.4, 29.7. FT-IR ( $\nu_{max}$ ,  $cm^{-1}$ ): 3297 (NH), 3094 (CH, aromatic). ESI-MS,  $m/z$ : 440.4  $[M+H]^+$ . HRMS (ESI,  $m/z$ ) calcd for  $C_{21}H_{16}ON_7F_3$   $[M+H]^+$  440.1441, found 440.1445.

#### 4.1.6.24.

*1-methyl-5-((1-methyl-1H-pyrazolo[3,4-d]pyrimidin-4-yl)oxy)-N-(4-(trifluoromethyl)phenyl)-1H-benzo[d]imidazol-2-amine (9s)*

Compound **7b** (0.2 g, 0.74 mmol) was reacted with 4-(trifluoromethyl)phenyl isothiocyanate (0.150 g, 0.74 mmol) to give **9s** as a white solid (0.125 g, yield: 38.5%). mp: 271-274 °C.  $^1H$  NMR (400 MHz, DMSO- $d_6$ )  $\delta$  9.48 (s, 1H), 8.54 (s, 1H), 8.08 (d,  $J$  = 8.8 Hz, 2H), 7.80 (s, 1H), 7.69 (d,  $J$  = 8.8 Hz, 2H), 7.45 (d,  $J$  = 8.8 Hz, 1H), 7.39 (d,  $J$  = 2.0 Hz, 1H), 7.05 (dd,  $J$  = 8.4, 2.4 Hz, 1H), 4.03 (s, 3H), 3.81 (s, 3H).  $^{13}C$  NMR (101 MHz, DMSO- $d_6$ )  $\delta$  164.4, 155.5, 155.3, 151.2, 147.4, 144.7, 142.3, 132.8, 131.4, 126.3, 117.9, 114.4, 110.2, 109.2, 102.2, 34.4, 29.8. FT-IR ( $\nu_{max}$ ,  $cm^{-1}$ ): 3344 (NH), 3098 (CH, aromatic). ESI-MS,  $m/z$ : 440.4  $[M+H]^+$ . HRMS (ESI,  $m/z$ ) calcd. for  $C_{21}H_{16}ON_7F_3$   $[M+H]^+$  440.1441, found 440.1443.

#### 4.1.6.25.

*N-(4-methoxyphenyl)-1-methyl-5-((1-methyl-1H-pyrazolo[3,4-d]pyrimidin-4-yl)oxy)-1H-benzo[d]imidazol-2-amine (9t)*

Compound **7b** (0.2 g, 0.74 mmol) was reacted with 4-methoxyphenyl isothiocyanate (0.122 g,

0.74 mmol) to give **9t** as a white solid (0.117 g, yield: 39.3%). mp: 206-208 °C. <sup>1</sup>H NMR (400 MHz, DMSO-*d*<sub>6</sub>) δ 8.85 (s, 1H), 8.53 (s, 1H), 7.76 (d, *J* = 8.8 Hz, 2H), 7.71 (s, 1H), 7.35 (d, *J* = 8.4 Hz, 1H), 7.26 (s, 1H), 6.91-6.97 (m, 3H), 4.02 (s, 3H), 3.73 (s, 6H). <sup>13</sup>C NMR (101 MHz, DMSO-*d*<sub>6</sub>) δ 164.5, 155.5, 155.3, 154.6, 152.8, 147.2, 143.0, 134.2, 133.1, 131.4, 120.4, 114.3, 113.2, 109.5, 108.4, 102.1, 55.6, 34.4, 29.5, 26.7. FT-IR (ν<sub>max</sub>, cm<sup>-1</sup>): 3316 (NH), 3094 (CH, aromatic). ESI-MS, *m/z*: 402.5 [M+H]<sup>+</sup>. HRMS (ESI, *m/z*) calcd. for C<sub>21</sub>H<sub>19</sub>O<sub>2</sub>N<sub>7</sub> [M+H]<sup>+</sup> 402.1673; found, 402.1675.

#### 4.1.6.26.

*1-methyl-5-((1-methyl-1H-pyrazolo[3,4-d]pyrimidin-4-yl)oxy)-N-(4-(trifluoromethoxy)phenyl)-1H-benzimidazol-2-amine (9u)*

Compound **7b** (0.2 g, 0.74 mmol) was reacted with 4-(trifluoromethoxy)phenyl isothiocyanate (0.162 g, 0.74 mmol) to give **9u** as a white solid (0.134 g, yield: 39.7%). mp: 240-242 °C. <sup>1</sup>H NMR (400 MHz, DMSO-*d*<sub>6</sub>) δ 9.25 (s, 1H), 8.53 (s, 1H), 7.98 (d, *J* = 8.8 Hz, 2H), 7.77 (s, 1H), 7.41 (d, *J* = 8.4 Hz, 1H), 7.33-7.35 (m, 3H), 7.01 (dd, *J* = 8.4, 2.0 Hz, 1H), 4.03 (s, 3H), 3.78 (s, 3H). <sup>13</sup>C NMR (101 MHz, DMSO-*d*<sub>6</sub>) δ 164.4, 155.5, 155.3, 151.8, 147.3, 142.5, 140.4, 132.9, 131.4, 122.0, 119.5, 114.0, 110.0, 108.9, 102.2, 34.4, 29.7. FT-IR (ν<sub>max</sub>, cm<sup>-1</sup>): 3290 (NH), 3099 (CH, aromatic). ESI-MS, *m/z*: 456.5 [M+H]<sup>+</sup>. HRMS (ESI, *m/z*) calcd. for C<sub>21</sub>H<sub>16</sub>O<sub>2</sub>N<sub>7</sub>F<sub>3</sub> [M+H]<sup>+</sup> 456.1390; found, 456.1395.

#### 4.1.6.27.

*N-benzyl-1-methyl-5-((1-methyl-1H-pyrazolo[3,4-d]pyrimidin-4-yl)oxy)-1H-benzimidazol-2-amine (9v)*

Compound **7b** (0.2 g, 0.74 mmol) was reacted with benzyl isothiocyanate (0.110 g, 0.74 mmol) to give **9v** as a white solid (0.049 g, yield: 17.1%). mp: 156-158 °C. <sup>1</sup>H NMR (400MHz, DMSO-*d*<sub>6</sub>) δ 8.59(s, 1H), 8.02(s, 1H), 7.51(s, 1H), 7.28-7.31(m, 4H), 7.17-7.23(m, 1H), 7.06(d, *J* = 8.4 Hz, 1H), 6.70(d, *J* = 2.8 Hz, 1H), 6.52(dd, *J* = 2.4, 8.4 Hz, 1H), 5.31(s, 2H), 4.04(s, 3H), 3.46(s, 3H). <sup>13</sup>C NMR (101MHz, DMSO-*d*<sub>6</sub>) δ 182.8, 163.3, 155.5, 155.3, 152.7, 146.2, 140.2, 131.5, 129.8, 128.4, 127.3, 126.7, 110.2, 108.8, 102.2, 48.7, 34.4. FT-IR (ν<sub>max</sub>, cm<sup>-1</sup>): 3321 (NH), 3032 (CH, aromatic), 2940 (CH, aliphatic). ESI-MS, *m/z*: 386.4 [M+H]<sup>+</sup>. HRMS (ESI, *m/z*) calcd. for C<sub>21</sub>H<sub>19</sub>ON<sub>7</sub> [M+H]<sup>+</sup> 386.1724; found, 386.1726 .

#### 4.1.6.28.

*N-(4-methoxybenzyl)-1-methyl-5-((1-methyl-1H-pyrazolo[3,4-d]pyrimidin-4-yl)oxy)-1H-benzimidazol-2-amine*

*zol-2-amine (9w)*

Compound **7b** (0.2 g, 0.74 mmol) was reacted with benzyl isothiocyanate (0.132 g, 0.74 mmol) to give **9w** as a white solid (0.048 g, yield: 15.8%). mp: 197-199 °C. <sup>1</sup>H NMR (400 MHz, DMSO-*d*<sub>6</sub>) δ 8.52(s, 1H), 7.67(s, 1H), 7.32-7.38(m, 3H), 7.23(d, *J* = 8.4 Hz, 1H), 7.09(d, *J* = 2.0 Hz, 1H), 6.89(d, *J* = 8.4 Hz, 2H), 6.84(dd, *J* = 8.4, 2.0 Hz, 1H), 4.53(d, *J* = 6.0 Hz, 2H), 4.02(s, 3H), 3.73(s, 3H), 3.58(s, 3H). <sup>13</sup>C NMR (101 MHz, DMSO-*d*<sub>6</sub>) δ 164.6, 158.6, 156.7, 155.5, 155.3, 146.9, 134.0, 132.4, 131.4, 129.0, 114.0, 112.1, 108.7, 107.7, 102.1, 55.4, 45.6, 34.4, 28.9. FT-IR (ν<sub>max</sub>, cm<sup>-1</sup>): 3451 (NH), 3236 (CH, aromatic), 2921 (CH, aliphatic). ESI-MS, *m/z*: 416.5 [M+H]<sup>+</sup>. HRMS (ESI, *m/z*) calcd. for C<sub>22</sub>H<sub>21</sub>O<sub>2</sub>N<sub>7</sub>[M+H]<sup>+</sup> 416.1830; found, 416.1832.

4.1.6.29. 5-((1-ethyl-1H-pyrazolo[3,4-*d*]pyrimidin-4-yl)oxy)-1-methyl-N-(4-(trifluoromethoxy)phenyl)-1H-benzo[*d*]imidazol-2-amine (**10a**)

Compound **7c** (0.2 g, 0.70 mmol) was reacted with 4-(trifluoromethoxy)phenyl isothiocyanate (0.153 g, 0.70 mmol) to give **10a** as a white solid (0.100 g, yield: 28.9%). mp: 256-258 °C. <sup>1</sup>H NMR (400 MHz, DMSO-*d*<sub>6</sub>) δ 9.26(s, 1H), 8.53(s, 1H), 7.99(d, *J* = 9.2 Hz, 2H), 7.77(s, 1H), 7.42(d, *J* = 8.4 Hz, 1H), 7.33-7.35(m, 3H), 7.02(dd, *J* = 2.4, 8.4 Hz, 1H), 4.46(q, *J* = 7.2 Hz, 2H), 3.78(s, 3H), 1.42(t, *J* = 7.2 Hz, 3H). <sup>13</sup>C NMR (101 MHz, DMSO-*d*<sub>6</sub>) δ 164.4, 155.4, 154.8, 151.8, 147.3, 142.5, 140.4, 132.9, 131.5, 122.0, 119.5, 114.0, 110.0, 108.9, 102.2, 42.4, 29.7, 15.1. FT-IR (ν<sub>max</sub>, cm<sup>-1</sup>): 3295 (NH), 3106 (CH, aromatic), 2924 (CH, aliphatic). ESI-MS, *m/z*: 470.4 [M+H]<sup>+</sup>. HRMS (ESI, *m/z*) calcd. for C<sub>22</sub>H<sub>18</sub>O<sub>2</sub>N<sub>7</sub>F<sub>3</sub>[M+H]<sup>+</sup> 470.1548; found, 470.1550.

4.1.6.30. 5-((1-ethyl-1H-pyrazolo[3,4-*d*]pyrimidin-4-yl)oxy)-1-methyl-N-(*p*-tolyl)-1H-benzo[*d*]imidazol-2-amine (**10b**)

Compound **7c** (0.2 g, 0.70 mmol) was reacted with 4-methylphenyl isothiocyanate (0.110 g, 0.70 mmol) to give **10b** as a white solid (0.072 g, yield: 24.5%). mp: 238-240 °C. <sup>1</sup>H NMR (400 MHz, DMSO-*d*<sub>6</sub>) δ 8.91(s, 1H), 8.53(s, 1H), 7.72-7.76(m, 3H), 7.37(d, *J* = 8.4 Hz, 1H), 7.30(s, 1H), 7.14(d, *J* = 8.0 Hz, 2H), 6.98(dd, *J* = 1.6, 8.4 Hz, 1H), 4.46(q, *J* = 7.2 Hz, 2H), 3.76(s, 3H), 2.27(s, 3H), 1.42(t, *J* = 7.2 Hz, 3H). <sup>13</sup>C NMR (101 MHz, DMSO-*d*<sub>6</sub>) δ 164.5, 155.4, 154.8, 152.4, 147.2, 142.9, 138.6, 133.0, 131.5, 130.4, 129.4, 118.7, 113.5, 109.7, 108.6, 102.2, 42.4, 29.6, 20.8, 15.1. FT-IR (ν<sub>max</sub>, cm<sup>-1</sup>): 3289 (NH), 3083 (CH, aromatic), 2919 (CH, aliphatic). ESI-MS, *m/z*: 400.4 [M+H]<sup>+</sup>. HRMS (ESI, *m/z*)

calcd. for  $C_{22}H_{21}ON_7$   $[M+H]^+$  400.1881; found, 400.1883.

4.1.6.31. *N*-(4-chloro-3-(trifluoromethyl)phenyl)-5-((1-ethyl-1*H*-pyrazolo[3,4-*d*]pyrimidin-4-yl)oxy)-1-methyl-1*H*-benzo[*d*]imidazol-2-amine (**10c**)

Compound **7c** (0.2 g, 0.70 mmol) was reacted with 4-chloro-3-(trifluoromethyl)phenyl isothiocyanate (0.166 g, 0.70 mmol) to give **10c** as a white solid (0.091 g, yield: 26.7%). mp: 277-279 °C.  $^1H$  NMR (400 MHz, DMSO- $d_6$ )  $\delta$  9.54(s, 1H), 8.53(s, 1H), 8.42(s, 1H), 8.32(d,  $J$  = 8.8 Hz, 1H), 7.79(s, 1H), 7.68(d,  $J$  = 8.8 Hz, 1H), 7.45(d,  $J$  = 8.8 Hz, 1H), 7.06(dd,  $J$  = 1.2, 8.4 Hz, 1H), 4.46(q,  $J$  = 7.2 Hz, 2H), 3.80(s, 3H), 1.43(t,  $J$  = 7.2 Hz, 3H).  $^{13}C$  NMR (101 MHz, DMSO- $d_6$ )  $\delta$  164.4, 155.4, 154.8, 151.2, 147.4, 142.3, 140.6, 132.7, 132.3, 131.4, 122.7, 114.4, 110.3, 109.2, 102.3, 42.4, 29.7, 15.0. FT-IR ( $\nu_{max}$ ,  $cm^{-1}$ ): 3283 (NH), 3085 (CH, aromatic), 2911 (CH, aliphatic). ESI-MS,  $m/z$ : 488.5  $[M+H]^+$ . HRMS (ESI,  $m/z$ ) calcd. for  $C_{22}H_{17}ON_7ClF_3$   $[M+H]^+$  488.1208; found, 488.1211.

4.1.6.32.

*N*-(4-bromophenyl)-5-((1-ethyl-1*H*-pyrazolo[3,4-*d*]pyrimidin-4-yl)oxy)-1-methyl-1*H*-benzo[*d*]imidazol-2-amine (**10d**)

Compound **7c** (0.2 g, 0.70 mmol) was reacted with 4-bromophenyl isothiocyanate (0.150 g, 0.70 mmol) to give **10d** as a white solid (0.095 g, yield: 29.3%). mp: 248-250 °C.  $^1H$  NMR (400 MHz, DMSO- $d_6$ )  $\delta$  9.19(s, 1H), 8.53(s, 1H), 7.89(d,  $J$  = 8.4 Hz, 2H), 7.75(s, 1H), 7.50(d,  $J$  = 8.4 Hz, 1H), 7.41(d,  $J$  = 8.4 Hz, 1H), 7.35(s, 1H), 7.02(dd,  $J$  = 1.2, 8.4 Hz, 1H), 4.45(q,  $J$  = 7.2 Hz, 2H), 3.78(s, 3H), 1.42(t,  $J$  = 7.2 Hz, 3H).  $^{13}C$  NMR (101 MHz, DMSO- $d_6$ )  $\delta$  164.4, 155.4, 154.8, 151.7, 147.3, 142.6, 140.5, 132.8, 131.7, 131.4, 120.3, 114.0, 112.9, 110.0, 108.9, 102.2, 42.4, 29.7, 15.1. FT-IR ( $\nu_{max}$ ,  $cm^{-1}$ ): 3284 (NH), 3099 (CH, aromatic), 2913 (CH, aliphatic). ESI-MS,  $m/z$ : 465.3  $[M+H]^+$ . HRMS (ESI,  $m/z$ ) calcd. for  $C_{21}H_{18}ON_7Br$   $[M+H]^+$  464.0830; found, 464.0833.

4.1.6.33.

5-((1-isopropyl-1*H*-pyrazolo[3,4-*d*]pyrimidin-4-yl)oxy)-1-methyl-*N*-(4-(trifluoromethoxy)phenyl)-1*H*-benzo[*d*]imidazol-2-amine (**11a**)

Compound **7d** (0.2 g, 0.67 mmol) was reacted with 4-(trifluoromethoxy)phenyl isothiocyanate (0.147 g, 0.67 mmol) to give **11a** as a white solid (0.083 g, yield: 25.7%). mp: 235-237 °C.  $^1H$  NMR (400 MHz, DMSO- $d_6$ )  $\delta$  9.26(s, 1H), 8.52(s, 1H), 7.98(d,  $J$  = 9.2 Hz, 2H), 7.75(s, 1H), 7.42(d,  $J$  = 8.4

Hz, 1H), 7.34-7.35(m, 3H), 7.02(dd,  $J = 2.0, 8.4$  Hz, 1H), 5.10-5.17(m, 1H), 3.78(s, 3H), 1.50(d,  $J = 6.8$  Hz, 6H).  $^{13}\text{C}$  NMR (101 MHz, DMSO- $d_6$ )  $\delta$  164.4, 155.2, 154.3, 151.8, 147.3, 142.5, 140.4, 132.9, 131.3, 122.0, 119.5, 114.0, 110.0, 108.9, 102.3, 49.4, 29.7, 22.2. FT-IR ( $\nu_{\text{max}}$ ,  $\text{cm}^{-1}$ ): 3304 (NH), 3099(CH, aromatic), 2943 (CH, aliphatic). ESI-MS,  $m/z$ : 484.6[M+H] $^+$ . HRMS (ESI,  $m/z$ ) calcd. for  $\text{C}_{23}\text{H}_{20}\text{ON}_7\text{F}_3$  [M+H] $^+$  484.1704; found, 484.1705.

#### 4.1.6.34.

5-((1-isopropyl-1H-pyrazolo[3,4-d]pyrimidin-4-yl)oxy)-1-methyl-N-(p-tolyl)-1H-benzo[d]imidazol-2-amine (**11b**)

Compound **7d** (0.2 g, 0.67 mmol) was reacted with 4-methylphenyl isothiocyanate (0.100 g, 0.67 mmol) to give **11b** as a white solid (0.059 g, yield: 21.3%). mp: 234-236 °C.  $^1\text{H}$  NMR (400 MHz, DMSO- $d_6$ )  $\delta$  8.91(s, 1H), 8.52(s, 1H), 7.75(d,  $J = 8.4$  Hz, 2H), 7.70(s, 1H), 7.37(d,  $J = 8.4$  Hz, 1H), 7.3(d,  $J = 2.4$  Hz, 1H), 7.14(d,  $J = 8.4$  Hz, 2H), 6.98(dd,  $J = 2.4, 8.4$  Hz, 1H), 5.10-5.17(m, 1H), 3.75(s, 3H), 3.75(s, 3H), 1.50(d,  $J = 6.8$  Hz, 6H).  $^{13}\text{C}$  NMR (101 MHz, DMSO- $d_6$ )  $\delta$  164.5, 155.2, 154.3, 152.4, 147.2, 142.9, 138.5, 133.0, 131.3, 130.4, 129.4, 118.6, 113.5, 109.7, 108.6, 102.3, 49.3, 29.6, 22.2, 20.8. FT-IR ( $\nu_{\text{max}}$ ,  $\text{cm}^{-1}$ ): 3305 (NH), 3089 (CH, aromatic), 2921 (CH, aliphatic). ESI-MS,  $m/z$ : 414.6[M+H] $^+$ . HRMS (ESI,  $m/z$ ) calcd. for  $\text{C}_{23}\text{H}_{24}\text{ON}_7$  [M+H] $^+$  414.2037; found, 414.2040.

#### 4.1.6.35.

N-(4-chloro-3-(trifluoromethyl)phenyl)-5-((1-isopropyl-1H-pyrazolo[3,4-d]pyrimidin-4-yl)oxy)-1-methyl-1H-benzo[d]imidazol-2-amine (**11c**)

Compound **7d** (0.2 g, 0.67 mmol) was reacted with 4-chloro-3-(trifluoromethyl)phenyl isothiocyanate (0.159 g, 0.67 mmol) to give **11c** as a white solid (0.089 g, yield: 26.6%). mp: 271-273 °C.  $^1\text{H}$  NMR (400 MHz, DMSO- $d_6$ )  $\delta$  9.54(s, 1H), 8.52(s, 1H), 8.42(d,  $J = 2.4$  Hz, 1H), 8.31(dd,  $J = 2.8, 9.2$  Hz, 1H), 7.77(s, 1H), 7.68(d,  $J = 8.8$  Hz, 1H), 7.45(d,  $J = 8.8$  Hz, 1H), 7.39(d,  $J = 2.0$  Hz, 1H), 7.06(dd,  $J = 2.0, 8.4$  Hz, 1H), 5.10-5.17(m, 1H), 3.80(s, 3H), 1.50(d,  $J = 6.8$  Hz, 6H).  $^{13}\text{C}$  NMR (101 MHz, DMSO- $d_6$ )  $\delta$  164.4, 155.2, 154.3, 151.1, 147.4, 142.3, 140.6, 132.7, 132.3, 131.2, 127.1, 124.7, 122.7, 121.7, 117.0, 114.4, 110.4, 109.2, 102.4, 99.9, 49.4, 29.7, 22.2. FT-IR ( $\nu_{\text{max}}$ ,  $\text{cm}^{-1}$ ): 3329 (NH), 3103 (CH, aromatic), 2967 (CH, aliphatic). ESI-MS,  $m/z$ : 502.6[M+H] $^+$ . HRMS (ESI,  $m/z$ ) calcd. for  $\text{C}_{23}\text{H}_{19}\text{ON}_7\text{ClF}_3$  [M+H] $^+$  502.1365; found, 502.1367.

## 4.1.6.36.

*N*-(4-bromophenyl)-5-((1-isopropyl-1*H*-pyrazolo[3,4-*d*]pyrimidin-4-yl)oxy)-1-methyl-1*H*-benzo[*d*]imidazol-2-amine (**11d**)

Compound **7d** (0.2 g, 0.67 mmol) was reacted with 4-bromophenyl isothiocyanate (0.143 g, 0.67 mmol) to give **11d** as a white solid (0.094 g, yield: 29.4%). mp: 235-237 °C. <sup>1</sup>H NMR (400 MHz, DMSO-*d*<sub>6</sub>) δ 9.19(s, 1H), 8.52(s, 1H), 7.88(d, *J* = 8.8 Hz, 2H), 7.74(s, 1H), 7.50(d, *J* = 8.8 Hz, 2H), 7.41(d, *J* = 8.4 Hz, 1H), 7.35(d, *J* = 2.0 Hz, 1H), 7.02(dd, *J* = 2.0, 8.4 Hz, 1H), 5.10-5.17(m, 1H), 3.77(s, 3H), 1.50(d, *J* = 6.4 Hz, 6H). <sup>13</sup>C NMR (101 MHz, DMSO-*d*<sub>6</sub>) δ 164.4, 155.2, 154.3, 151.7, 147.3, 142.6, 140.5, 132.8, 131.7, 131.3, 120.3, 114.0, 112.9, 110.0, 108.9, 102.3, 49.3, 29.7, 22.2. FT-IR (ν<sub>max</sub>, cm<sup>-1</sup>): 3257 (NH), 3095 (CH, aromatic), 2972 (CH, aliphatic). ESI-MS, *m/z*: 478.6[M+H]<sup>+</sup>. HRMS (ESI, *m/z*) calcd. for C<sub>22</sub>H<sub>20</sub>ON<sub>7</sub>Br [M+H]<sup>+</sup> 478.0986; found, 478.0988.

4.1.7. 4-(4-(benzyloxy)phenoxy)-1-methyl-1*H*-pyrazolo[3,4-*d*]pyrimidine (**12**)

Compound **4a** (2.0 g, 11.9 mmol) was reacted with 4-(benzyloxy)phenol (2.38 g, 11.9 mmol) according to general procedure B to give **12** (3.2 g, yield: 82.6%). <sup>1</sup>H NMR (400 MHz, CDCl<sub>3</sub>) δ 8.59(s, 1H), 7.81(s, 1H), 7.37-7.42(m, 5H), 7.20(d, *J* = 8.8 Hz, 2H), 7.09(d, *J* = 8.8 Hz, 2H), 5.12(s, 3H), 4.14(s, 3H). ESI-MS, *m/z*: 333.7 [M+H]<sup>+</sup>.

4.1.8. 4-((1-methyl-1*H*-pyrazolo[3,4-*d*]pyrimidin-4-yl)oxy)phenol (**13**)

A solution of **12** (1.0 g, 3.0 mmol) in TFA (10 mL) was stirred for 20 h at 50 °C. Then the mixture was cooled to rt, basified with the saturated aqueous NaHCO<sub>3</sub> (50 mL), and extracted with EtOAc. The organic layer was washed with water and brine, dried over Na<sub>2</sub>SO<sub>4</sub>, filtered, and concentrated *in vacuo*. The crude residue was purified by recrystallization 95% ethanol to give **13** as white needles (0.546 g, yield: 75.3%). <sup>1</sup>H NMR (400 MHz, DMSO-*d*<sub>6</sub>) δ 9.60(s, 1H), 8.53(s, 1H), 7.89(s, 1H), 7.11(d, *J* = 8.8 Hz, 2H), 6.85(d, *J* = 8.8 Hz, 2H), 4.03(s, 3H). ESI-MS, *m/z*: 243.5 [M+H]<sup>+</sup>.

4.1.9. 4-((1-methyl-1*H*-pyrazolo[3,4-*d*]pyrimidin-4-yl)oxy)-2-nitrophenol (**14**)

To a flask charged with **13** (1.0 g, 4.13 mmol) in AcOH (20 mL), fuming HNO<sub>3</sub> (0.26 g, 4.13 mmol) was added dropwise. The reaction mixture was stirred at rt for 40 min, after that saturated aqueous NaHCO<sub>3</sub> (50 mL) was poured slowly. Then the reaction mixture was extracted with CH<sub>2</sub>Cl<sub>2</sub>,

washed with water and brine, dried over  $\text{Na}_2\text{SO}_4$ , filtered, and concentrated *in vacuo*. The residue was purified by silica gel column chromatography using a petroleum ether-EtOAc to yield **14** as orange solid (0.612 g yield: 51.6%).  $^1\text{H}$  NMR (400 MHz,  $\text{DMSO-}d_6$ )  $\delta$  11.15(s, 1H), 8.57(s, 1H), 8.29(s, 1H), 7.93(d,  $J = 3.2$  Hz, 2H), 6.85(dd,  $J = 3.2, 8.8$  Hz, 1H), 7.24(d,  $J = 9.2$  Hz, 1H), 4.07(s, 3H). ESI-MS,  $m/z$ : 288.5  $[\text{M}+\text{H}]^+$ .

#### 4.1.10. 2-amino-4-((1-methyl-1H-pyrazolo[3,4-d]pyrimidin-4-yl)oxy)phenol (**15**)

Compound **14** (1.5 g, 5.23 mmol) was reacted with hydrazine hydrate (1.26 mL, 26 mmol) according to general procedure D to give **15** (0.921 g, yield: 68.5%).  $^1\text{H}$  NMR (400 MHz,  $\text{DMSO-}d_6$ )  $\delta$  9.23(s, 1H), 8.55(s, 1H), 7.60(s, 1H), 6.70(d,  $J = 8.4$  Hz, 1H), 6.48(d,  $J = 2.8$  Hz, 1H), 6.30(dd,  $J = 2.8, 8.4$  Hz, 1H), 4.82(s, 2H), 4.01(s, 3H). ESI-MS,  $m/z$ : 258.5  $[\text{M}+\text{H}]^+$ .

#### 4.1.11. 5-((1-methyl-1H-pyrazolo[3,4-d]pyrimidin-4-yl)oxy)-N-(4-(trifluoromethoxy)phenyl)benzo[d]oxazol-2-amine (**16a**)

Compound **15** (0.2 g, 0.78 mmol) was reacted with 4-(trifluoromethoxy)phenyl isothiocyanate (0.171 g, 0.78 mmol) according to the general procedure E to give **16a** as a white solid (0.095 g, yield: 27.6%). mp: 243-245 °C.  $^1\text{H}$  NMR (400 MHz,  $\text{DMSO-}d_6$ )  $\delta$  10.98(s, 1H), 8.56(s, 1H), 8.08(s, 1H), 7.87(d,  $J = 8.4$  Hz, 2H), 7.61(d,  $J = 8.4$  Hz, 1H), 7.40-7.46(m, 3H), 7.10(d,  $J = 8.8$  Hz, 1H), 4.06(s, 3H).  $^{13}\text{C}$  NMR (101 MHz,  $\text{DMSO-}d_6$ )  $\delta$  163.8, 159.4, 155.4, 155.3, 149.0, 145.4, 143.7, 143.4, 138.3, 131.4, 122.4, 119.4, 115.8, 111.0, 109.9, 102.2, 34.5. FT-IR ( $\nu_{\text{max}}$ ,  $\text{cm}^{-1}$ ): 3228 (NH), 3033 (CH, aromatic). ESI-MS,  $m/z$ : 441.3  $[\text{M}-\text{H}]^-$ . HRMS (ESI,  $m/z$ ) calcd. for  $\text{C}_{20}\text{H}_{13}\text{O}_3\text{N}_6\text{F}_3$   $[\text{M}+\text{H}]^+$  443.1074; found, 443.1075.

#### 4.1.12. 5-((1-methyl-1H-pyrazolo[3,4-d]pyrimidin-4-yl)oxy)-N-(p-tolyl)benzo[d]oxazol-2-amine (**16b**)

Compound **15** (0.2 g, 0.78 mmol) was reacted with 4-methylphenyl isothiocyanate (0.116 g, 0.78 mmol) according to the general procedure E to give **16b** as a white solid (0.071 g, yield: 24.5%). mp: 222-224 °C.  $^1\text{H}$  NMR (400 MHz,  $\text{DMSO-}d_6$ )  $\delta$  10.64(s, 1H), 8.56(s, 1H), 8.05(s, 1H), 7.64(d,  $J = 8.4$  Hz, 2H), 7.57(d,  $J = 8.4$  Hz, 1H), 7.42(d,  $J = 2.4$  Hz, 1H), 7.19(d,  $J = 8.0$  Hz, 2H), 7.05(dd,  $J = 2.4, 8.8$  Hz, 1H), 4.05(s, 3H), 2.28(s, 3H).  $^{13}\text{C}$  NMR (101 MHz,  $\text{DMSO-}d_6$ )  $\delta$  163.9, 159.7, 155.4, 155.3, 149.0, 145.4, 144.1, 136.4, 131.7, 131.4, 129.8, 118.2, 115.3, 110.7, 109.6, 102.2, 34.4, 20.8. FT-IR ( $\nu_{\text{max}}$ ,  $\text{cm}^{-1}$ ): 3313 (NH), 3038 (CH, aromatic). ESI-MS,  $m/z$ : 371.7  $[\text{M}-\text{H}]^-$ . HRMS (ESI,  $m/z$ ) calcd.

for  $C_{20}H_{16}O_2N_6$   $[M+H]^+$  373.1409; found, 373.1411 .

#### 4.1.13.

*N*-(4-chloro-3-(trifluoromethyl)phenyl)-5-((1-methyl-1*H*-pyrazolo[3,4-*d*]pyrimidin-4-yl)oxy)benzo[*d*]oxazol-2-amine (**16c**)

Compound **15** (0.2 g, 0.78 mmol) was reacted with 4-chloro-3-(trifluoromethyl)phenyl isothiocyanate (0.185 g, 0.78mmol) according to the general procedure E to give **16c** as a red solid (0.096 g, yield: 26.8%). mp: 200-202 °C.  $^1H$  NMR (400 MHz, DMSO- $d_6$ )  $\delta$  11.26(s, 1H), 8.56(s, 1H), 8.28(d,  $J = 2.8$  Hz, 1H), 8.06-8.09(m, 2H), 7.76(d,  $J = 8.8$  Hz, 1H), 7.65(d,  $J = 8.8$  Hz, 1H), 7.52(d,  $J = 2.4$  Hz, 1H), 7.13(dd,  $J = 2.4, 8.4$  Hz, 1H), 4.06(s, 3H).  $^{13}C$  NMR (101 MHz, DMSO- $d_6$ )  $\delta$  163.8, 158.9, 155.4, 155.3, 149.1, 145.3, 143.3, 138.5, 132.8, 131.4, 123.3, 122.8, 116.7, 116.3, 111.4, 110.1, 102.2, 34.5. FT-IR ( $\nu_{max}$ ,  $cm^{-1}$ ): 3256 (NH), 3066 (CH, aromatic); ESI-MS,  $m/z$ : 459.4  $[M-H]^-$ . HRMS (ESI,  $m/z$ ) calcd. for  $C_{20}H_{12}O_2N_6F_3Cl$   $[M+H]^+$  461.0737; found, 461.0738 .

#### 4.1.14.

*N*-(4-bromophenyl)-5-((1-methyl-1*H*-pyrazolo[3,4-*d*]pyrimidin-4-yl)oxy)benzo[*d*]oxazol-2-amine (**16d**)

Compound **15** (0.2 g, 0.78 mmol) was reacted with 4-bromophenyl isothiocyanate (0.167 g, 0.78mmol) according to the general procedure E to give **16d** as an orange solid (0.088 g, yield: 25.7%). mp: 274-276 °C.  $^1H$  NMR (400 MHz, DMSO- $d_6$ )  $\delta$  10.9(s, 1H), 8.56(s, 1H), 8.08(s, 1H), 7.74(d,  $J = 8.4$  Hz, 1H), 7.57-7.62(m, 3H), 7.46(s, 1H), 7.09(d,  $J = 9.2$  Hz, 1H), 4.06(s, 3H).  $^{13}C$  NMR (101 MHz, DMSO- $d_6$ )  $\delta$  163.8, 159.2, 155.4, 155.3, 149.0, 145.3, 143.7, 138.3, 132.2, 131.4, 120.0, 115.8, 114.3, 111.0, 109.8, 102.2, 34.5. FT-IR ( $\nu_{max}$ ,  $cm^{-1}$ ): 3341 (NH), 2966 (CH, aromatic); ESI-MS,  $m/z$ : 437.4  $[M-H]^-$ . HRMS (ESI,  $m/z$ ) calcd. for  $C_{19}H_{13}O_2N_6Br$   $[M+H]^+$  437.0357; found, 437.0360.

#### 4.2 Kinase inhibitory activity

The BRAF<sup>V600E</sup> and VEGFR-2 inhibitory activity was evaluated by using the Z'-LYTE technology platform (Life Technologies), and Sorafenib was employed as the positive control. The experiments were performed according to the instructions of the manufacturer, and single point concentration tested with two independent data points ( $n = 2$ ). We chose compounds with high percent inhibition values to evaluate kinase activity at ten concentration gradients from 1000 to 0.0508 nM

(3-fold dilution). The  $IC_{50}$  values were calculated from the inhibition curves from two separate experiments.

#### 4.3 Cell proliferation inhibition assay

The anti-proliferative activities of compounds were evaluated against A375, HT-29, and HUVEC cell lines by the standard MTT assay *in vitro*, with Sorafenib as the positive control. All cell lines were purchased from Cell Bank of China Science Academy (Shanghai, China). All chemicals and solvents were purchased from Sigma-Aldrich or Gibco. The A375 and H-29 cell lines were maintained in DEME and RPMI 1640 medium supplement, respectively, with 10% fetal bovine serum (FBS) and 1% Penicillin-Streptomycin, while the HUVEC cell line was maintained in F-12k medium supplement with 10% fetal bovine serum (FBS), 1% Penicillin-Streptomycin, 50  $\mu\text{g}/\text{mL}$  heparin and 0.03-0.05  $\text{mg}/\text{mL}$  ECGS. Approximate  $5 \times 10^3$  cells, suspended in medium, were plated into each well of a 96-well plate and grown at  $37^\circ\text{C}$  in a humidified atmosphere with 5%  $\text{CO}_2$  for 24 h. The following day various concentrations of tested compounds were added to the culture medium and incubated for 72 h. Fresh MTT was added to each well at the terminal concentration of 5  $\text{mg}/\text{mL}$  in PBS, and incubated with cells at  $37^\circ\text{C}$  for 4 h. The formazan crystals in each well were dissolved in 150  $\mu\text{L}$  DMSO, and the absorbency at 570 nm was measured with an enzyme-linked immunosorbent assay plate reader. All of the compounds were tested three times in each of the cell lines.

#### 4.4 Flow-activating cell sorting analysis

The effect of compound **9u** on cell cycle phase distribution of A375 was assessed using flow cytometry. When the cells grew to about 70 % confluence in 6-well microplates, they were treated with compound **9u** at given concentrations (0.87, 1.74, 3.48  $\mu\text{mol}/\text{L}$ ). After 48 h, cells were harvested by trypsinization, washed with PBS, and fixed in 70 % ice cold (4 $^\circ\text{C}$ ) ethanol overnight. They were then washed with PBS, incubated with RNase (50  $\text{mg}/\text{mL}$  final concentration) at  $37^\circ\text{C}$  for 30 min, stained with propidium iodide (50  $\text{mg}/\text{mL}$  final concentration), and analyzed by flow cytometry (BD FACSCanto II). HUVEC cell line was treated with **9u** at given concentration (2.95, 5.89, 11.78  $\mu\text{mol}/\text{L}$ ) with the same procedure as A375 cell line.

#### 4.5 Molecular Modeling

Docking study was performed on Glide module of Schrödinger suite (New York, NY) [46]. The crystal structures of BRAF<sup>V600E</sup> (PDB ID: 1UWJ) [45] and VEGFR-2 (PDB ID: 3WZE [34]) in complex with Sorafenib were retrieved from the Protein Databank Bank (<http://www.rcsb.org/>). Before starting the docking, the protein structures were prepared and minimized using the protein preparation wizard of Schrödinger. Hydrogen atoms were added, proper bond orders were assigned, missing side chains were generated using prime module while the protonation states of each side chain were generated using Epik at pH = 7. Protein minimization was performed with the default cutoff root mean square deviation (RMSD) value of 0.3 Å using Optimized Potentials for Liquid Simulations (OPLS) 2005 force field. The ligands were prepared using the Ligprep module of the Schrödinger Suite. These prepared structures were used for molecular docking studies. Protein receptor grid was generated at the center of cocrystallized inhibitor sorafenib active site region using Receptor grid generation with a 1.0 van der Waals radius scaling factor and 0.25 partial charge cut-off without any constraint. Once the receptor grid is generated, the **9u** was docked to the protein using Glide “Extra precision mode” (XP). The best docking configurations based on the Glide scores (G-scores) were selected as the most probable binding conformation and were subjected to molecular dynamics simulation.

The MD simulations were performed using AMBER 12 software package (San Francisco, USA) [47-48] according to our previously published protocol [49-50]. Geometry optimization and the electrostatic potential calculations for **9u** was carried out at the HF/6-31G\* level of the Gaussian 09 suite [51]. The atomic partial charge was obtained by using the restrained electrostatic potential (RESP) fitting technique [52] implemented in AmberTools [53]. The force field parameters for **9u** and Sorafenib were generated by the general amber force field (GAFF) [54] using the Antechamber program. The AMBER 99SB force field [55] was used to simulate the protein structure and the ionization states of amino acid residues were set according to the standard protocol. The model was neutralized by adding suitable counterions and were solvated in a truncated octahedron box of the transferable interaction potential (TIP3P) [56] water molecules with a margin distance of 12 Å. The fully solvated and neutralized system was subjected to energy minimization. Following minimization, the system was gradually heated from 0 to 300 K in 50 ps using a Langevin thermostat with a coupling coefficient of 1.0/ps with a force constant  $2.0 \text{ kcal}\cdot\text{mol}^{-1}\cdot\text{Å}^{-2}$  on the complex. Then, 50 ps of density equilibration with a force constant  $2.0 \text{ kcal}\cdot\text{mol}^{-1}\cdot\text{Å}^{-2}$  on the complex was performed. Subsequently the

systems were again equilibrated for 500 ps by releasing all the restraints. Finally, the 50-ns MD production was performed at 300 K with 1.0 atm pressure. During the MD simulations, the long-range Coulombic interactions were handled using the particle mesh Ewald (PME) method [57]. The cutoff distance for the long-range vdW energy term was set at 10.0 Å. Periodic boundary conditions were applied to avoid edge effects in all calculations. The SHAKE algorithm [58] was employed on all atoms covalently bond to hydrogen atoms, allowing for an integration time step of 2 fs. Coordinate trajectories were recorded every 10 ps throughout all equilibration and production runs. The binding-free energies ( $\Delta G_{\text{bind}}$ ) were calculated by using MM-GBSA and MM-PBSA [59-60] procedure in AMBER12. Average 1000 snapshots were extracted from the last 10 ns MD trajectory for the calculations, and only 10 snapshots evenly extracted from the last 10 ns MD trajectory were used to calculate the entropic contribution.

#### Acknowledgments:

This work was supported by grants from the National Natural Science Foundation of China (No. 81202413 and 81573263), Natural Science Foundation of Guangdong Province, China (No. 2015A030313285) and the Science and Technology Planning Project of Guangdong Province, China (No. 2014A020210012).

#### References

- [1] Y. Sun, W.Z. Liu, T. Liu, X. Feng, N. Yang, H.F. Zhou. Signaling pathway of MAPK/ERK in cell proliferation, differentiation, migration, senescence and apoptosis. *J. Recept. Signal Transduct. Res.* 35 (2015) 600-604
- [2] D.X. Liu, X. Liu, M.Z. Xing, Epigenetic genes regulated by the BRAF<sup>V600E</sup> signaling are associated with alterations in the methylation and expression of tumor suppressor genes and patient survival in melanoma, *Biochem. Biophys. Res. Commun.* 425 (2012) 45–50.
- [3] S. Rocca, G. Carrà, P. Poggio, A. Morotti, M. Brancaccio. Targeting few to help hundreds: JAK, MAPK and ROCK pathways as druggable targets in atypical chronic myeloid leukemia. *Mol Cancer.* (2018):40
- [4] A. Vultur, J. Villanueva, M. Herlyn, Targeting BRAF in advanced melanoma: a first step toward manageable disease, *Clin. Cancer Res.* 17 (2011) 1658–1663.

- [5] J. Mooz, T.K. Oberoi-Khanuja, G.S. Harms, W. Wang, B.S. Jaiswal, S. Seshagiri, R. Tikkanen, K. Rajalingam, Dimerization of the kinase ARAF promotes MAPK pathway activation and cell migration, *Sci. Signal.* 7 (2014) ra73.
- [6] A.P. Rebocho, R. Marais, New insight puts CRAF in sight as a therapeutic target, *Cancer Discov.* 1 (2011) 98-99.
- [7] A.P. Rebocho, R. Marais. ARAF acts as a scaffold to stabilize BRAF: CRAF heterodimers, *Oncogene* 32 (2013) 3207-3212.
- [8] I. Tusa, S. Gagliardi, A. Tubita, S. Pandolfi, C. Urso, L. Borgognoni, J. Wang, X. Deng, N.S. Gray, B. Stecca, E. Rovida, ERK5 is activated by oncogenic BRAF and promotes melanoma growth, *Oncogene*, 37 (2018) 2601-2614.
- [9] H. Davies, G.R. Bignell, C. Cox, P. Stephens, S. Edkins, S. Clegg, J. Teague, H. Woffendin, M.J. Garnett, W. Bottomley, N. Davis, E. Dicks, R. Ewing, Y. Floyd, K. Gray, S. Hall, R. Hawes, J. Hughes, V. Kosmidou, A. Menzies, C. Mould, A. Parker, C. Stevens, S. Watt, S. Hooper, R. Wilson, H. Jayatilake, B.A. Gustereson, C. Cooper, J. Shipley, D. Hargrave, K. Pritchard-Jones, N. Maitland, G. Chenevix-Trench, G.J. Riggins, D.D. Bigner, G. Palmieri, A. Cossu, A. Flanagan, A. Nicholson, J.W.C. Ho, S.Y. Leung, S.T. Yuen, B.L. Weber, H.F. Seigler, T.L. Darrow, H. Paterson, R. Marais, C.J. Marshall, R. Wooster, M.R. Stratton, P.A. Futreal, Mutations of the BRAF gene in human cancer, *Nature* 417 (2002) 949-954.
- [10] J.M. Motherwell, C.R. Anderson, W.L. Murfee, Endothelial cell phenotypes are maintained during angiogenesis in cultured microvascular networks, *Sci. Rep.* 8(2018) 5887.
- [11] J. Folkman, Angiogenesis: an organizing principle for drug discovery? *Nat. Rev. Drug Discov.* 6 (2007) 273-286.
- [12] S.M. Abou-Seri, W.M. Eldehna, M.M. Ali, D.A.A.E. Ella, 1-Piperazinylphthalazines as potential VEGFR-2 inhibitors and anticancer agents: synthesis and in vitro biological evaluation. *Eur. J. Med. Chem.* 107 (2016) 165-179.
- [13] L. Shi, T.T. Wu, Z. Wang, J.Y. Xue, Y.G. Xu, Discovery of quinazolin-4-amines bearing benzimidazole fragments as dual inhibitors of c-Met and VEGFR-2, *Bioorg. Med. Chem. Lett.* 22 (2014) 4735-4744.
- [14] S. Salerno, A.M. Marini, G. Fornaciari, F. Simorini, C.L. Motta, S. Taliani, S. Sartini, F.D. Settimo, A.N. Garcia-Argaez, O. Gia, S. Cosconati, E. Novellino, P. D'Ocon, A. Fioravanti, P. Orlandi, G.

- Bocci, L.D. Via, Investigation of new 2-aryl substituted benzothiopyrano[4,3-*d*]pyrimidines as kinase inhibitors targeting vascular endothelial growth factor receptor 2, *Eur. J. Med. Chem.* 103 (2015) 29-43.
- [15] F. Musumeci, M. Radi, C. Brullo, S. Schenone, Vascular endothelial growth factor (VEGF) Receptors: drugs and new inhibitors, *J. Med. Chem.* 55 (2012) 10797-10822.
- [16] H.P. Gao, P. Su, Y.L. Shi, X.X. Shen, Y.M. Zhang, J.Y. Dong, J. Zhang, Discovery of novel VEGFR-2 inhibitors. Part II: biphenyl urea incorporated with salicylaldehyde, *Eur. J. Med. Chem.* 90 (2015) 232-240.
- [17] A. Alavi, J.D. Hood, R. Frausto, D.G. Stupack, D.A. Cheresh, Role of Raf in vascular protection from distinct apoptotic stimuli, *Science* 301 (2003) 94-96.
- [18] J.D. Hood, M. Bednarski, R. Frausto, S. Guccione, R.A. Reisfeld, R. Xiang, D.A. Cheresh, Tumor regression by targeted gene delivery to the neovasculature, *Science* 296 (2002) 2404-2407.
- [19] S.M. Wilhelm, C. Carter, L.Y. Tang, D. Wilkie, A. McNabola, H. Rong, C. Chen, X.M. Zhang, P. Vincent, M. McHugh, Y.C. Cao, J. Shujath, S. Gawlak, D. Eveleigh, B. Rowley, L. Liu, L. Adnane, M. Lynch, D. Auclair, I. Taylor, R. Gedrich, A. Voznesensky, B. Riedl, L.E. Post, G. Bollag, P.A. Trail, BAY 43-9006 exhibits broad spectrum oral antitumor activity and targets the RAF/MEK/ERK pathway and receptor tyrosine kinases involved in tumor progression and angiogenesis, *Cancer Res.* 64 (2004) 7099-7109.
- [20] Food and Drug Administration. Highlights of Prescribing Information. [http://www.accessdata.fda.gov/drugsatfda\\_docs/label/2007/021923s004s005s006s007lbl.pdf](http://www.accessdata.fda.gov/drugsatfda_docs/label/2007/021923s004s005s006s007lbl.pdf) (accessed Jan 11, 2012).
- [21] T. Eisen, T. Ahmad, K.T. Flaherty, M. Gore, S. Kaye, R. Marais, I. Gibbens, S. Hackett, M. James, L.M. Schuchter, K.L. Nathanson, C. Xia, R. Simantov, B. Schwartz, M. Poulin-Costello, P.J. O'Dwyer, M.J. Ratain, Sorafenib in advanced melanoma: a phase II randomised discontinuation trial analysis, *Brit. J. Cancer* 95 (2006) 581-586.
- [22] E. Venetsanakos, D. Stuart, N. Tan, H. Ye, F. Salangsang, K. Aardalen, M. Faure, C. Heise, D. Mendel, B. Jallal, CHIR-265, a novel inhibitor that targets B-Raf and VEGFR, shows efficacy in a broad range of preclinical models, *Proc. Amer. Assoc. Cancer Res.* 47 (2006) 4854
- [23] Y. Liu, N.S. Gray, Rational design of inhibitors that bind to inactive kinase conformations, *Nat. Chem. Biol.* 2 (2006) 358-364.
- [24] A.C. Backes, B. Zech, B. Felber, B. Klebl, G. Müller, Small molecule inhibitors binding to protein

- kinase. Part II: The novel pharmacophore approach of type II and type III inhibition, *Expert Opin. Drug Discov.* 3 (2008) 1427–1449.
- [25] G. Bollag, J. Tsai, J. Zhang, C. Zhang, P. Ibrahim, K. Nolop, P. Hirth, Vemurafenib: the first drug approved for BRAF-mutant cancer, *Nat. Rev. Drug Discov.* 11(2012) 873-886
- [26] G.P. Bollag, J. Hirth, J. Tsai, P.N. Zhang, H. Ibrahim, W. Cho, C. Spevak, Y. Zhang, G. Zhang, G. Habets, E.A. Burton, B. Wong, G. Tsang, B.L. West, B. Powell, R. Shellooe, A. Marimuthu, H. Nguyen, K.Y. Zhang, D.R. Artis, J. Schlessinger, F. Su, B. Higgins, R. Iyer, K. D'Andrea, A. Koehler, M. Stumm, P.S. Lin, R.J. Lee, J. Grippo, I. Puzanov, K.B. Kim, A. Ribas, G.A. McArthur, J.A. Sosman, P.B. Chapman, K.T. Flaherty, X. Xu, K.L. Nathanson, K. Nolop, Clinical efficacy of a RAF inhibitor needs broad target blockade in BRAF-mutant melanoma, *Nature* 467 (2010) 596–599.
- [27] P.B. Chapman, A. Hauschild, C. Robert, J.B. Haanen, P. Ascierto, J. Larkin, R. Dummer, C. Garbe, A. Testori, M. Maio, D. Hogg, P. Lorigan, C. Lebbe, T. Jouary, D. Schadendorf, A. Ribas, S.J. O'Day, J.A. Sosman, J.M. Kirkwood, A.M.M. Eggermont, B. Dreno, K. Nolop, J. Li, B. Nelson, J. Hou, R.J. Lee, K.T. Flaherty, G.A. McArthur, Improved survival with vemurafenib in melanoma with BRAF<sup>V600E</sup> mutation, *N. Engl. J. Med.* 364 (2011) 2507–2516.
- [28] A. Hauschild, J.J. Grob, L.V. Demidov, T. Jouary, R. Gutzmer, M. Millward, P. Rutkowski, C.U. Blank, W.H. Miller, E. Kaempgen, S. Martín-Algarra, B. Karaszewska, C. Mauch, V. Chiarion-Sileni, A.M. Martin, S. Swann, P. Haney, B. Mirakhur, M.E. Guckert, V. Goodman, P.B. Chapet, Dabrafenib in BRAF mutated metastatic melanoma: A multicentre, open-label, phase 3 randomised controlled trial, *Lancet* 380 (2012) 358–365.
- [29] R.M. Anforth, T.C.M.P. Blumetti, R.F. Kefford, R. Sharma, R.A. Scolyer, S. Kossard, G.V. Long, P. Fernandez-Peñas, Cutaneous manifestations of dabrafenib (GSK2118436): A selective inhibitor of mutant BRAF in patients with metastatic melanoma, *Brit. J. Dermatol.* 167 (2012) 1153–1160.
- [30] G.S. Falchook, G.V. Long, R. Kurzrock, K.B. Kim, T.H. Arkenau, M.P. Brown, O. Hamid, J.R. Infante, M. Millward, A.C. Pavlick, S.J. O'Day, S.C. Blackman, C.M. Curtis, P. Lebowitz, B. Ma, D. Ouellet, R.F. Kefford, Dabrafenib in patients with melanoma, untreated brain metastases, and other solid tumours: A phase 1 dose-escalation trial, *Lancet* 379 (2012) 1893–1901.
- [31] K.T. Flaherty, I. Puzanov, K.B. Kim, A. Ribas, G.A. McArthur, J.A. Sosman, P.J. O'Dwyer, R.J. Lee, J.F. Grippo, K. Nolop, P.B. Chapman, Inhibition of mutated, activated BRAF in metastatic

- melanoma, *N. Engl. J. Med.* 363 (2010) 809–819.
- [32] J. Blanc, R. Geney, C. Menet, Type II kinase inhibitors: an opportunity in cancer for rational design, *Anti-cancer Agents Med. Chem.* 13 (2013) 731-747.
- [33] Y. Fu, Y. Wang, S. Wan, Z. Li, G. Wang, J. Zhang, X. Wu, Bisarylureas based on 1*H*-pyrazolo[3,4-*d*]pyrimidine scaffold as novel pan-RAF inhibitors with potent anti-proliferative activities: structure-based design, synthesis, biological evaluation and molecular modelling studies, *Molecules* 22 (2017) 542.
- [34] K. Okamoto, M. Ikemori-Kawada, A. Jestel, K. Konig, Y. Funahashi, T. Matsushima, A. Tsuruoka, A. Inoue, J. Matsui, Distinct binding mode of multikinase inhibitor lenvatinib revealed by biochemical characterization. *ACS Med. Chem. Lett.* 6 (2015) 89-94
- [35] R. A. Friesner, R. B. Murphy, M. P. Repasky, L. L. Frye, J. R. Greenwood, T. A. Halgren, P. C. Sanschagrin, D. T. Mainz, Extra precision Glide: docking and scoring incorporating a model of hydrophobic enclosure for protein–ligand complexes. *J. Med. Chem.* 49(2006) 6177-6196.
- [36] T. A. Halgren, R. B. Murphy, R. A. Friesner, H. S. Beard, L. L. Frye, W. T. Pollard, J. L. Banks, Glide: A new approach for rapid, accurate docking and scoring. 2. Enrichment factors in database screening, *J. Med. Chem.* 47(2004)1750-1759.
- [37] R. A. Friesner, J. L. Banks, R. B. Murphy, T. A. Halgren, J. J. Klicic, D. T. Mainz, M. P. Repasky, E. H. Knoll, M. Shelley, J. K. Perry, D. E. Shaw, P. Francis, P. S. Shenkin, Glide: A new approach for rapid, accurate docking and scoring. 1. method and assessment of docking accuracy, *J. Med. Chem.* 47(2004)1739-1749.
- [38] S. P. Kasturi, S. Surarapu, S. Uppalanchi, S. Dwivedi, P. Yogeewari, D.K. Sigalapalli, N.B. Bathini, K.S. Ethiraj, J.S. Anireddy, Synthesis, molecular modeling and evaluation of  $\alpha$ -glucosidase inhibition activity of 3,4-dihydroxy piperidines. *Eur. J. Med. Chem.* 150 (2018) 39-52
- [39] D. F. Veber, S. R. Johnson, H.-Y. Cheng, B. R. Smith, K.W. Ward, K.D. Kopple, Molecular properties that influence the oral bioavailability of drug candidates. *J. Med. Chem.* 45 (2002) 2615-2623.
- [40] H. Michele, J. Bready, A. Coxon, M. Thomas, Jr. DeMelfi, L. DiPietro, N. Doerr, D. Elbaum, J. Estrada, P. Gallant, J. Germain, Y. Gu, J.C. Harmange, S.A. Kaufman, R. Kendall, J.L. Kim, G.N. Kumar, A.M. Long, S. Neervannan, V.F. Patel, A. Polverino, P. Rose, P. Simon van der, D.

- Whittington, R. Zanon, H.L. Zhao. Design, synthesis, and evaluation of orally active benzimidazoles and benzoxazoles as vascular endothelial growth factor-2 receptor tyrosine Kinase inhibitors, *J. Med. Chem.* 50 (2007) 4351-4373.
- [41] A. Ghavanini, Comment on: MTT assay instead of the clonogenic assay in measuring the response of cells to ionizing, *J. Radiobiol.* 1(2014) 15-16.
- [42] E. Mccullagh, A. Seshan, H. Elsamad, H.D. Madhani, Coordinate control of gene expression noise and interchromosomal interactions in a MAP kinase pathway, *Nat. Cell. Biol.* 12 (2010) 954-962.
- [43]G. Luo, Z. Tang , K. Lao, X. Li, Q. You, H. Xiang. Structure-activity relationships of 2,4-disubstituted pyrimidines as dual ER $\alpha$ /VEGFR-2 ligands with anti-breast cancer activity. *Eur. J. Med. Chem.* 150 (2018) 783-795
- [44]R. Singla, K. B. Gupta, S. Upadhyay, M. Dhiman, V. Jaitak. Design, synthesis and biological evaluation of novel indolebenzimidazole hybrids targeting estrogen receptor alpha (ER- $\alpha$ ). *Eur. J. Med. Chem.* 146 (2018) 206-219
- [45] P.T.C. Wan, M.J. Garnett, S.M. Roe, S. Lee, D. Niculescu-Duvaz, V.M Good, C.M Jones, C.J. Marshall, C.J. Springer, D. Barford, R. Marais, Mechanism of Activation of the RAF-ERK Signaling Pathway by Oncogenic Mutations of B-RAF. *Cell* 116 (2004) 855-867.
- [46] Schrödinger **Release** 2017-1, Schrödinger LLC, New York, NY, 2017.
- [47] D.A. Case, T.A. Darden, T.E. Cheatham III, C.L. Simmerling, J. Wang, R.E. Duke, R. Luo, R.C. Walker, W. Zhang, K.M. Merz, B. Roberts, S. Hayik, A. Roitberg, G. Seabra, J. Swails, A.W. Goetz, I. Kolossváry, K.F. Wong, F. Paesani, J. Vanicek, R.M. Wolf, J. Liu, X. Wu, S.R. Brozell, T. Steinbrecher, H. Gohlke, Q. Cai, X. Ye, J. Wang, M.J. Hsieh, G. Cui, D.R. Roe, D.H. Mathews, M.G. Seetin, R. Salomon-Ferrer, C. Sagui, V. Babin, T. Luchko, S. Gusarov, A. Kovalenko, P.A. Kollman, AMBER 12, 2012, University of California, San Francisco.
- [48] R. Salomon-Ferrer, A.W. Götz, D. Poole, S. Le Grand, R.C. Walker, Routine microsecond molecular dynamics simulations with AMBER on GPUs. 2. Explicit solvent particle mesh Ewald. *J. Chem. Theory Comput.* 9 (2013) 3878–3888.
- [49] X. Wu, S. Wan, G. Wang, H. Jin, Z. Li, Y. Tian, Z. Zhu, J. Zhang, Molecular dynamics simulation and free energy calculation studies of kinase inhibitors binding to active and inactive conformations of VEGFR-2. *J. Mol. Graph. Model.* 56 (2015) 103-112.
- [50] Y. Tian, T. Zhang, L. Long, Z. Li, S. Wan, G. Wang, Y. Yu, J. Hou, X. Wu, J. Zhang, Design,

- synthesis, biological evaluation and molecular modeling of novel 2-amino-4-(1-phenylethoxy) pyridine derivatives as potential ROS1 inhibitors, *Eur J Med Chem*, 143(2018)182-199.
- [51] M.J. Frisch, G.W. Trucks, H.B. Schlegel, G.E. Scuseria, M.A. Robb, J.R. Cheeseman, G. Scalmani, V. Barone, B. Mennucci, G.A. Petersson, H. Nakatsuji, M. Caricato, X. Li, H.P. Hratchian, A.F. Izmaylov, J. Bloino, G. Zheng, J.L. Sonnenberg, M. Hada, M. Ehara, K. Toyota, R. Fukuda, J. Hasegawa, M. Ishida, T. Nakajima, Y. Honda, O. Kitao, H. Nakai, T. Vreven, J. A. Montgomery, Jr., J.E. Peralta, F. Ogliaro, M. Bearpark, J.J. Heyd, E. Brothers, K. N. Kudin, V.N. Staroverov, R. Kobayashi, J. Normand, K. Raghavachari, A. Rendell, J.C. Burant, S.S. Iyengar, J. Tomasi, M. Cossi, N. Rega, J.M. Millam, M. Klene, J.E. Knox, J.B. Cross, V. Bakken, C. Adamo, J. Jaramillo, R. Gomperts, R.E. Stratmann, O. Yazyev, A.J. Austin, R. Cammi, C. Pomelli, J.W. Ochterski, R.L. Martin, K. Morokuma, V.G. Zakrzewski, G.A. Voth, P. Salvador, J.J. Dannenberg, S. Dapprich, A.D. Daniels, Ö. Farkas, J.B. Foresman, J.V. Ortiz, J. Cioslowski, D.J. Fox, Gaussian 09, Gaussian, Inc., Wallingford, CT., 2009
- [52] C.I. Bayly, P. Cieplak, W. Cornell, P.A. Kollman, A well-behaved electrostatic potential based method using charge restraints for deriving atomic charges: The RESP model. *J. Phys. Chem.* 97 (1993) 10269–10280.
- [53] J. Wang, W. Wang, P.A. Kollman, D.A. Case, Automatic atom type and bond type perception in molecular mechanical calculations. *J. Mol. Graph. Model* 25 (2006) 247–260.
- [54] J. Wang, R.M. Wolf, J.W. Caldwell, P.A. Kollman, D.A. Case, Development and testing of a general amber force field. *J. Comput. Chem.* 25 (2004) 1157–1174.
- [55] K. Lindorff-Larsen, S. Piana, K. Palmo, P. Maragakis, J.L. Klepeis, R.O. Dror, Improved side-chain torsion potentials for the Amber ff99SB protein force field. *Proteins Struct. Funct. Bioinform.* 78 (2010) 1950-1958.
- [56] W.L. Jorgensen, J. Chandrasekhar, J.D. Madura, R.W. Impey, M.L. Klein, Comparison of simple potential functions for simulating liquid water, *J. Chem. Phys.* 79 (1983) 926–935.
- [57] T. Darden, D. York, L. Pedersen, Particle mesh Ewald: An  $N \cdot \log(N)$  method for Ewald sums in large systems. *J. Chem. Phys.* 98 (1993) 10089–10092.
- [58] J.P. Ryckaert, G. Ciccotti, H.J. Berendsen, Numerical integration of the cartesian equations of motion of a system with constraints: Molecular dynamics of *n*-alkanes. *J. Comput. Phys.* 23 (1977) 327–341.

- [59] P.A. Kollman, I. Massova, C. Reyes, B. Kuhn, S. Huo, L. Chong, M. Lee, T. Lee, Y. Duan, W. Wang, Calculating structures and free energies of complex molecules: Combining molecular mechanics and continuum models. *Acc. Chem. Res.* 33 (2000) 889–897.
- [60] G. Rastelli, R.A. Del, G. Degliesposti, M. Sgobba, Fast and accurate predictions of binding free energies using MM-PBSA and MM-GBSA. *J. Comput. Chem.* 31 (2010) 797-810.

### Highlights

- A series of 1*H*-pyrazolo[3,4-*d*]pyrimidine derivatives were designed and synthesized as BRAF<sup>V600E</sup> and VEGFR-2 dual inhibitors.
- The compound **9u** exhibited potent inhibitory activities against BRAF<sup>V600E</sup> and VEGFR-2, and potent anti-proliferative activity against BRAF<sup>V600E</sup>-expressing A375 and H-29 as well as VEGFR-2-expressing HUVEC, respectively.
- Molecular simulations gave a probable molecular explanation for the activity of compound **9u**.
- The structures of compounds are novel and expand the chemical diversity of BRAF<sup>V600E</sup> and VEGFR-2 dual inhibitors.